Detecting vegetation stress in mixed forest ecosystems through the joint use of tree-water monitoring and land surface modeling

C.D. Jiménez-Rodríguez[1], G. Fabiani[1], R. Schoppach[1], K. Mallick[1], S.J. Schymanski[1], and M. Sulis[1]

[1]Environmental Research and Innovation (ERIN) Department, Luxembourg Institute of Science and Technology (LIST), Belvaux, L-4422, Luxembourg.

Corresponding author: César Jiménez-Rodríguez (cdjimenezcr@gmail.com)

Key Points:

- We show that the model's dominant fraction of a mixed ecosystem masks the water status of smaller fractions within a grid cell.
- We demonstrate that refining the plant hydraulic traits based on species presence improves the representation of mixed forests in CLM5.
- We evidence the limitations of CLM5 in reproducing the needleleaf water stress using tree water deficit measurements.

Abstract

Recent European heatwaves have significantly impacted forest ecosystems, leading to increased plant water stress. Advances in land surface models aim to improve the representation of vegetation drought responses by incorporating plant hydraulics into the plant functional type (PFT) classification system. However, reliance on PFTs may inadequately capture the diverse plant hydraulic traits (PHTs), potentially biasing transpiration and vegetation water stress representations. The detection of vegetation drought stress is further complicated by the mixing of different tree species and forest patches. This study uses the Community Land Model version 5.0 to simulate an experimental mixed-forest catchment with configurations representing standalone, patched mixed, and fully-mixed forests. Biome-generic, PFT-specific, or species-specific PHTs are employed. Results emphasize the crucial role of accurately representing mixed forests in reproducing observed vegetation water stress and transpiration fluxes for both broadleaf and needleleaf tree species. The dominant vegetation fraction is a key determinant, influencing aggregated vegetation response patterns. Segregation level in PHT parameterizations shapes differences between observed and simulated transpiration fluxes. Simulated root water potential emerges as a potential metric for detecting vegetation stress periods. However, the model's plant hydraulic system has limitations in reproducing the long-term effects of extreme weather events on needleleaf tree species. These findings highlight the complexity of modeling mixed forests and underscore the need for improved representation of plant diversity in land surface models to enhance the understanding of vegetation water stress under changing climate conditions.

Plain Language Summary

Numerical simulation models for large-scale ecosystems often oversimplify mixed forests, neglecting the diversity of species and structural complexity. This oversight impacts the accuracy of simulated plant water use, especially during droughts and heatwaves. This study focused on the specific traits of key tree species at a Luxembourg site, aiming to enhance the model's ability to represent the vegetation response to extreme conditions. By incorporating detailed plant traits, the model improved in replicating observed tree water use and identifying periods of water deficit. The findings highlight the importance of considering the functional diversity of mixed forest ecosystems for accurate simulations. Moreover, the study introduces a simple metric using the model's structure to pinpoint periods when different species experience severe water deficit. The proposed metric provides a practical tool for identifying critical periods of water stress for various species within mixed forests. This approach enhances our understanding of mixed forest dynamics under extreme conditions, emphasizing the need for nuanced representations in large-scale models.

1 Introduction

The increasing frequency and intensity of droughts and heatwaves in Europe pose challenges to vegetation (He et al., 2020), affecting various physiological processes (Arend et al., 2021; Hajek et al., 2022; Obladen et al., 2021; Senf et al., 2020). Dendrochronological studies indicate that coniferous trees (e.g., Spruce or European Larch) are generally more susceptible to drought than broadleaf trees (e.g., Beech or deciduous Oaks) (Vitasse et al., 2019). However, recent severe events, like the 2018 drought in central Europe, have endangered even the typically resilient Oak and Beech trees, with projections suggesting worsening conditions in the future (Schuldt et al.,

2020; Shekhar et al., 2024) . These extreme events disrupt the plant water transport system (Dietrich et al., 2019; Kannenberg, Novick, & Phillips, 2019; Tomasella et al., 2019), leading to constraints on carbon assimilation, delayed phenological development, and reduced plant growth. The negative effects of drought have lasting implications for a forest's long-term resilience to environmental changes. (Kannenberg et al., 2020; Van Passel et al., 2022). The combination of the duration of these impacts and the extent of disruption in physiological processes is termed as legacy effects. Recognizing and understanding these enduring consequences are crucial for assessing the overall health and adaptability of forest ecosystems in the face of evolving environmental conditions. (Kannenberg, Novick, Alexander, et al., 2019; Yu et al., 2022).

The responses of forest to changing environmental conditions is heavily influenced by tree competition (e.g., Fernández-de-Uña et al., 2015; Ford et al., 2017), where tree demography (e.g., size, age) and diversity (e.g., species) are the key features determining the individual tree interactions (Felton et al., 2010; Jactel et al., 2017; Pretzsch et al., 2013). Mixed forests, featuring multi-generational tree populations in the same area (del Río et al., 2018), exhibit structural complexity that enhances tree survival during prolonged droughts or heatwaves (Ma et al., 2023). The dynamic equilibrium in these ecosystems involves a balance between niche separation and resource competition among different tree species, with finite resources such as water, light, space, and nutrients influencing the vegetation response (Bravo-Oviedo et al., 2014). Resource competition among tree species in mixed forests is a dynamic process influenced by latitude, forest successional stage, and environmental conditions (McDowell et al., 2020). The intra-specific competition (Bosela et al., 2015) is amplified when environmental extremes, such as heatwaves and droughts occur, resulting in more frequent and massive die-off in the forests (Hammond et al., 2022). Furthermore, when exploring the effects of species mixing, site-dependent conditions like geology, species spatial distribution or forest successional stage must be taken into account (Gong et al., 2020; Han et al., 2022; Mina et al., 2018) to isolate the response related to species interactions from the effect of environmental factors.

The forest response to severe weather conditions, like heatwaves, has been monitored using remote sensing products that analyze long-term changes in land surface temperature, vegetation health index, or normalized difference vegetation index (e.g., Bento et al., 2020; Prăvălie et al., 2022). Although these products enable the simultaneous monitoring of large areas, their spatial resolution is inadequate to investigate physiological processes at the tree or organ level, such as stem dehydration. (e.g., stem dehydration). In this regard, in-situ measurements carried out with stem psychrometers, sap flow sensors, and tree dendrometers (e.g., Brinkmann et al., 2016; Guan et al., 2022; Mohanty et al., 2017; Zweifel et al., 2005) provide an inside view of multiple physiological aspects of the trees. Stem psychrometers measure water potential (Dixon & Tyree, 1984), revealing how plants respond to specific environmental stressors like droughts (Steppe, 2018). Sap flow sensors gauge sap velocity that can be upscaled to tree and stand transpiration (E_T) estimates (Poyatos et al., 2021). Tree dendrometers measure changes in tree diameter, allowing for the calculation of growth and the tree water deficit (TWD) (Zweifel et al., 2014). Therefore, the continuous monitoring of individual trees generates a detailed data set describing how the diverse forest tree population respond to harsh meteorological conditions that cannot be retrieved with remote sensing products.

Latest versions of land surface models (LSMs) have implemented a plant hydraulic system (PHS) to reproduce the water transport of the vegetation (e.g., Bonan et al., 2014; Eller et al., 2020; L. Li et al., 2021a), reduce the bias of soil-moisture based formulations of plant water stress (Sloan et al., 2021) and improve the simulated transpiration rates (e.g., Kennedy et al., 2019; L. Li et al., 2021a). The PHS uses the plant vulnerability curve (PVC) to characterize the hydraulic stress in the vegetation by describing plant hydraulic conductivity as a function of the water potential in a given plant organ (i.e., percent loss of hydraulic conductivity, PLC) (Venturas et al., 2017). The implementation of the PHS in LSMs allows to mimic the interspecific variability of plant transpiration response across forest stands and sites (e.g., (Jiménez-Rodríguez et al., 2024; Kennedy et al., 2019; Wu et al., 2020). Furthermore, the explicit simulation of the water potential in different plant segments (i.e., roots, stem, and leaves) provides the opportunity to compare the simulated plant water stress with novel measurements such as the TWD by exploiting experimental evidence on the link between tree diameters and water status (Dietrich et al., 2018; Schäfer et al., 2019).

The implementation of the PHS approach in LSMs relies on the homogenization of plant hydraulic traits (PHTs) for each plant functional type (PFT). The PFT classification uses a three-level system based on latitudinal location, phenology, and plant type (Colin Prentice et al., 1993) assuming homogeneous conditions for some biophysical variables of the forest (e.g., aerodynamic conductance). However, the use of the PFT classification system is currently under scrutiny due to its limitations in representing the functional diversity of forest ecosystems (Cranko Page et al., 2024). Therefore, the PHT parameterization of individual PFTs is a daunting task because the PHTs vary between individual trees and even more so between species of the same PFT (Domec et al., 2012; Hochberg et al., 2018; Rosner et al., 2019). This highly diverse nature of PHTs has become a major obstacle for PFT classification, highlighting the need to adopt alternative approaches (e.g., habitat filtering) where PHTs of different vegetation types are restricted according to trait-environment relationships (Chatanga & Sieben, 2020; Fry et al., 2019; Verheijen et al., 2015; Violle et al., 2014). In this regard, the use of the PFT classification to evaluate the PHS may be less problematic for mono-specific stands and more challenging for more complex ecosystems such as mixed forests that require a more detailed representation of their PHTs (Bohrer & Missik, 2022). For instance, in boreal mixed forests composed of Spruce and Birch species or in the Mesophytic deciduous forests dominated by Pedunculate Oak and Hornbeam (Barbati et al., 2014), there are examples in which the PHTs (e.g., Ψ_{p50}) of the main tree species differ considerably (Laughlin et al., 2023). This issue is further complicated in highly segregated landscapes where multiple PFTs, located within the same model grid cell, interact through the shared resources (e.g., soil water). While previous studies have tackled the challenge of representing sub-grid heterogeneity to understand the impacts of topographical gradients (Tesfa & Leung, 2017), hydrological processes (Torres-Rojas et al., 2022), or vegetation types (Ke et al., 2013) on the estimation of energy and water fluxes, no study has yet evaluated the impact of sub-grid heterogeneity on the simulated plant water stress in LSMs. In particular, the effect of homogenizing PHTs within single PFTs and/or across the landscape on the simulated plant water stress is still poorly understood.

This manuscript aims to assess the impact of standardizing the PHTs within the PFT classification system for diverse sub-grid representations of the landscape. The study investigates the transpiration and plant water status simulated by the advanced Land Surface Model, CLM5.0. It utilizes species- and region-specific PHTs, examining standalone, mixed patched, and fully-mixed forest stands. The underlying hypothesis suggests that a more detailed characterization of

PHTs in mixed forest ecosystems will better represent observed water fluxes and stress compared to the generic PFT generic parameterization. The study conducted a series of point-scale numerical experiments employing generic, PFT-specific, and species-specific plant hydraulic parameterizations. It considered both shared and separated access of forest stands to soil water resources. The research was conducted in the Weierbach catchment (Luxembourg), which has been extensively monitored in the last two decades (Hissler et al., 2021). The mixed forest cover of the Weierbach catchment allows for characterizing PHTs of two PFTs (i.e., broadleaf deciduous temperate trees (BDT) and needleleaf evergreen temperate trees (NET) and four tree species (i.e., Oak, Beech, Spruce, and Douglas fir). These species, representative of BDT and NET PFTs in Europe, have been monitored using sap flow and dendrometer sensors, providing information on the fluxes and plant water status under various weather conditions, including extreme weather events.

2 Materials and Methods

Forests in Europe cover 35% of the land area (FOREST EUROPE, 2020), and most of these stands are dominated by broadleaf deciduous (BDF) and needleleaf evergreen (NEF) forests (Poulter et al., 2015). The BDFs are represented mainly by Beech (*Fagus sylvatica* L.), Birch (*Betula* sp.), Hornbeam (*Carpinus betulus* L.), Maple (*Acer* sp.), and Oak (*Quercus* sp.) trees (de Rigo et al., 2016; Nascimbene et al., 2013). In Europe, the NEFs are mainly represented by Pine (*Pinus* sp.) and Spruce (*Picea* sp.) trees (Buras & Menzel, 2019; de Rigo et al., 2016) with commercial plantations of the non-native Douglas fir (*Pseudotsuga menziesii* (Mirbel) Franco) (Thomas et al., 2022). The Weierbach catchment in Luxembourg is covered by BDF and NEF forests, spatially distributed as mixed and standalone patches, respectively. The availability of continuous measurements of sap flow and tree diameters between 2019 and 2021 makes this case study suitable for evaluating the impact of the recent climate extremes on Europe's most representative forest types.

2.1. Study Site

The Weierbach catchment is located in the western part of Luxembourg (N: 49° 49’ 38”, E: 5° 47’ 44”), covering an area of 0.45 km^2, and an elevation range from 450 m a.s.l. to 500 m a.s.l. The catchment contributes to the Alzette river basin with a mean annual stream discharge of 478 mm yr^{-1} (Hissler et al., 2021). This catchment features a “V” shape topography and is located on top of a schist’s bedrock (Pfister et al., 2017), with a plateau feature on the upper catchment characterized by deep periglacial deposits and the hillslope with shallow soils (Martínez-Carreras et al., 2016). Soil characteristics in the plateau allow a larger storage capacity than in the shallow soils on the hillslope. The first 30 cm of soil have a silty clay texture, changing towards a loam texture at deeper layers (Glaser et al., 2016). The catchment has a semi-marine climate (Hissler et al., 2021) with a mean annual precipitation of 953 mm yr^{-1} and a mean annual temperature of 8.9 °C. The forested catchment is covered by a mixed deciduous forest of Beech (*Fagus sylvatica* L.*)* and Oak trees (mostly hybrids of *Quercus petraea* (Matt.) Liebl. and *Quercus robur* L.) covering 77.6% of the catchment, with the remaining 22.4% covered by small patches of coniferous stands of Spruce (*Picea abies* (L.) H. Karst.) and Douglas fir (*Pseudotsuga menziesii* (Mirbel) Franco) (Figure 1).

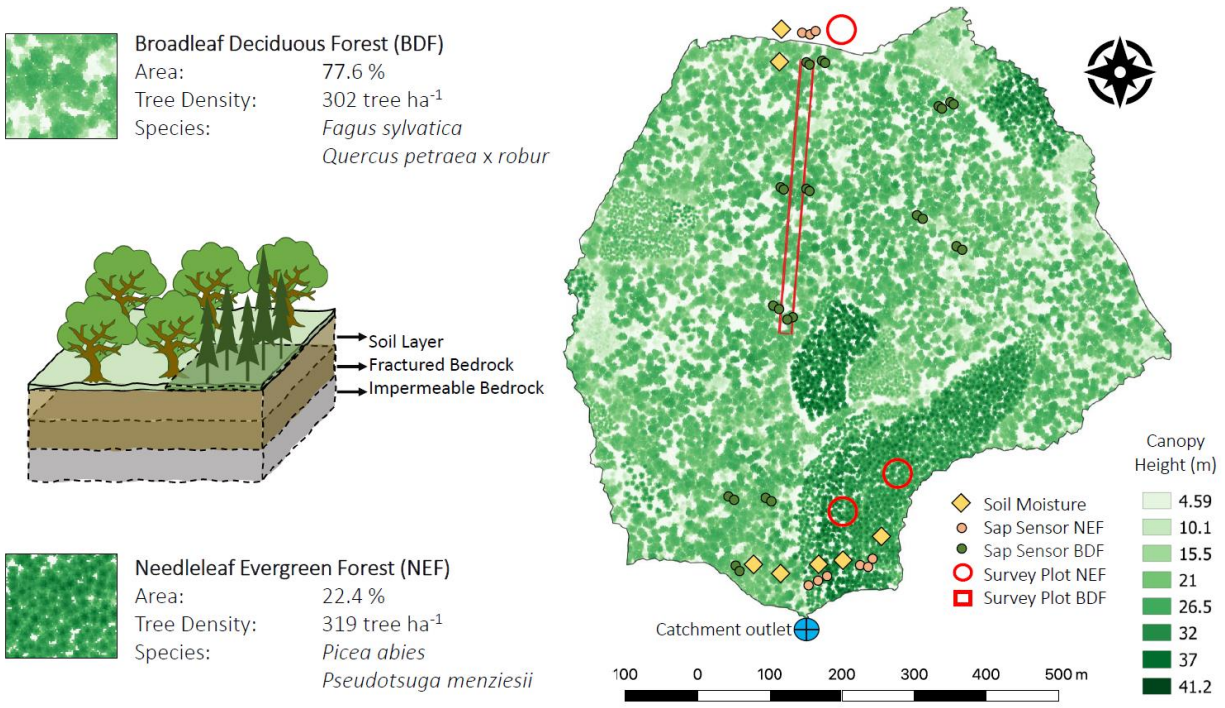

Figure 1. Map of the forested land cover at the Weierbach catchment obtained from the aerial LIDAR survey (ACT, 2020) describing the canopy height variation. The map also shows the spatial distribution of the environmental sensors (i.e., soil moisture, sap flow, and dendrometers) installed in the catchment. The schema on the left side of the figure represents the implementation of the catchment in the CLM5.0 modeling framework.

2.2 Transpiration estimates

Sap velocities (cm hr^{-1}) were measured in 13 Oak, 14 Beech, six Spruce, and three Douglas fir trees during the 2019 and 2020 growing season. Technical details of sensor deployment and calculation of sap velocities of the trees monitored at Weierbach can be found in Schoppach et al. (2021) and Fabiani et al., (2022). Sap flux per tree per cross sectional area (Q, $cm^3\ hr^{-1}$) was quantified by multiplying sap flow velocities by the sapwood area (cm^2) of each tree equipped with a sap flow sensor. The daily sap flux was calculated per tree ($m^3\ d^{-1}$) and averaged per species ($\overline{Q}$). The transpiration estimates (E_T) were calculated in mm d^{-1} based on Equation 1, where $\Lambda_{g.sp}$ is the basal area of the measured trees (m^2), $\Lambda_{G.sp}$ is the total basal area (m^2) of the species, Λ_r is the reference surface area (i.e., whole catchment or individual forest stand), and 1000 is the conversion factor from m to mm. The diameter class distribution and basal area was assessed with two surveys carried out with temporal plots in both forest types, the needleleaf evergreen and broadleaf deciduous stands (see Table S1).

$$E_T = \sum_{sp=1}^{n} 1000 \cdot \left(\frac{\overline{Q}}{\Lambda_{g.sp}}\right) \cdot \frac{\Lambda_{G.sp}}{\Lambda_r} \qquad \text{Equation 1}$$

2.3 Tree Water Deficit

The tree water deficit (TWD) was calculated based on tree diameter increment measurements on individual trees, carried out using high-resolution band dendrometers (model: DBL60 ICT) between 2019 and 2022. A total of 22 sensors were installed across the Weierbach catchment in nine Beech trees, nine Oak trees, three Spruce trees, and one Douglas fir tree. We selected the most representative trees from large (50–75 cm) and small (25–50 cm) diameter classes for Beech and Oak. Spruce and Douglas fir stands are evenly aged because they are a forest plantation. For this reason, we equipped trees from one diameter class only, ranging from 20 cm to 35 cm. The data was processed with the *treenetproc* R package (Haeni et al., 2020; Knüsel et al., 2021; Treenetproc, 2019/2023; Wickham et al., 2019), which allows the automated detection and removal of outliers. For each tree, we calculated the TWD, which is the difference between the theoretical radius at full hydration and the current radius (Zweifel et al., 2016). The tree water deficit of each forest type cover was determined using a weighted average of the species based on the area covered by each of them (see Table 2).

2.4 Model Setup

The Community Land Model version 5.0 (CLM5, Lawrence et al., (2019)) was implemented for the Weierbach catchment using a point-scale setup. Multi-year spin-up runs were performed until the soil moisture and temperature reached a dynamic equilibrium. Each spin-up covered a 11-year time window using the atmospheric forcing and land surface parameterization from 2011 to 2021. A production model run of the 11-year time window was carried-out after the spin-up period for each experiment; see section 2.5 and section 2.6 for additional details.

2.4.1 Atmospheric Forcing

Hourly atmospheric forcing was retrieved from the Roodt meteorological station (N: 49° 48’ 21.91”, E: 5° 49’52.49”), which is located 3.5 km south-east of the catchment. This data set includes precipitation (P) in mm hr^{-1}, wind speed (u) in m s^{-1}, air temperature (T) in °C, relative humidity (RH) in %, and incoming shortwave radiation (R_S) in W m^{-2}. To fill occasional gaps in T and P, we used the Aarsdorf (N: 49° 51’ 36.49”, E: 5° 50’32.9”) and Useldange stations (N: 49° 46’ 2.74”, E: 5° 58’2.17”). Gaps in atmospheric pressure (p) and downwelling longwave radiation (R_L) were filled using the ERA5 reanalysis product (Muñoz Sabater, 2019, 2021), downloaded from the Copernicus Climate Change Service (C3S) Climate Data Store. The atmospheric CO_2 concentration was kept constant at 411.6 ppm. This value is the average of daily measurements at Mauna Loa (NOAA-ESRL, 2022) between 2018 and 2022.

2.4.2 Soil and Bedrock Parameterization

The lower boundary condition describes the geopedological characteristics of the catchment, where soil texture and depth to bedrock are documented by Glaser et al. (2016). The clay content decreases with depth, from 45.2% (at 12 cm deep) to 22.27% below 32 cm deep. Meanwhile, the sand percentages increase considerably with depth, from 10% at the surface up to 31.41% below 32 cm (Table 1). The unsaturated zone at this site reaches down to 3.0 m where the soil Cv soil horizon is located. However, the default depth to bedrock used by CLM5 based

on Pelletier et al. (2016) is 95.4 cm at the Weierbach catchment making necessary to increase the unsaturated zone. Consequently, we modified the depth to bedrock by adding 150 cm and setting the clay and sand percentages of the newly added soil layers to 10.0% and 90.0%, respectively, following the approach proposed by Jiménez-Rodríguez et al. (2022a).

Table 1. Vertical distribution of the soil texture characterization used as the lower boundary condition for the numerical experiments carried out at the Weierbach catchment.

Depth [cm]	Description	Clay Fraction [%]	Sand Fraction [%]	Source
0 – 12	Soil Horizon Ah	45.20	10.04	(Glaser et al., 2016)
12 – 32	Soil Horizon Ah-B	37.70	16.04	(Glaser et al., 2016)
32 – 92	Soil Horizon B1/B2	22.27	31.41	(Glaser et al., 2016)
92 - 245	Weathered Bedrock	10.00	90.00	(Jiménez-Rodríguez et al. 2022a)

2.4.3 Land Surface Parameterization

The broadleaf deciduous (BDF) and needleleaf evergreen (NEF) forests were associated with the temperate plant functional type (PFT) broadleaf deciduous tree (BDT) and needleleaf evergreen tree (NET), respectively. The monthly leaf area index (LAI, m^2m^{-2}) of the BDT was determined based on MODIS (ORNL DAAC, 2018). The retrieved LAI is based on the mean value for the broadleaf deciduous classification of the 1.0 km area around the catchment boundaries, done using the MODISTools package (Hufkens, 2022; Tuck et al., 2014). The LAI of the BDT was set to 0 m^2m^{-2} between November and March to represent the dormant season. Default LAI values of CLM5 were used for the NET forest stand because MODIS does not correctly depict the signal due to the small sizes of needleleaf evergreen patches. To assess the proportion of Beech and Oak canopy to the total LAI, we employed the allometric equations from Pretzsch (2019) along with the data from the forest survey carried out in 2022 (Fabiani et al., 2022). We found that Oak and Beech contribute to 19.6% and 80.4%, respectively, of the total LAI of BDT (Text S1 and Figure S1).

2.4.4 Plant Hydraulic Parameterization

The plant hydraulic system (PHS) implemented in CLM5 aims to mimic the plant water transport in the model using Equation 2 to calculate the hydraulic conductance k ($mm_{H2O}\ mm_{H2O}^{-1}s^{-1}$) of each plant segment (i.e., roots, stem, and sunny and shaded leaves). Equation 2 represents the plant vulnerability curve (PVC) and uses the xylem pressure inducing 50% loss of hydraulic conductance (Ψ_{p50}, MPa), the non-dimensional sigmoidal shape parameter of the curve (c_k), the water potential of the lower segment (Ψ), and the maximum plant hydraulic conductance (k_{max}, $mm_{H2O}\ mm_{H2O}^{-1}s^{-1}$). Each of the plant hydraulic parameters (i.e., Ψ_{p50}, c_k, k_{max}) can be adjusted per plant segment and PFT and are considered static over time. In this study, we considered that the plant segments (i.e., roots, stems, leaves) within each PFT (and tree species classification) have the same plant hydraulic parameterization (i.e., k_{max}, Ψ_{p50}, and c_k).

$$k = k_{max} 2^{-\left(\frac{\Psi}{\Psi_{p50}}\right)^{c_k}} \quad \text{Equation 2}$$

CLM5 has a generic model parameterization (GMP) describing the main PFTs (Table 2). In this study, we created two additional parameterizations for the Weierbach forest stands. The PFT adjusted parameterization (PAP) describes the BDT and NET forest stands lumping the species present in each PFT fraction. The species-specific parameterization (SSP) characterizes the PHS of the individual tree species present in each forest fraction and do not lump the species per PFT. To determine the PHT parameters (i.e., Ψ_{p50} and c_k) of each additional parameterization (i.e., PAP and SSP), we sampled the Ψ_{p12}, Ψ_{p50}, and Ψ_{p88} values from the Xylem Functional Traits (XFT) database (Choat et al., 2012) for each tree species investigated. To improve the representation of Beech we did an additional search for PHT data, which resulted in an improved data set with 23 records (see Table S2). We followed the procedure described by Jiménez-Rodríguez et al. (2024) to determine the c_k used in the plant vulnerability curve of CLM5 for the mean Ψ_{p50} values of PAP and SSP (Table 1). Figures S2 and S3 show the differences in the PVCs of the different forest stand classification (i.e., BDT, NET, Oak, Beech, Spruce, Douglas fir) per parameterization (i.e., GMP, PAP, SSP).

Table 2. Plant hydraulic traits used for each model parameterization and forest stand. The percentage of land cover is estimated with respect to the catchment area. The area percentage value between brackets in Oak and Beech expresses the proportion of the BDT area covered by each species.

Parameterization	Forest Stand	Area [%]	Ψ_{p50} [MPa]	c_k
Generic Model Parameterization [GMP]	BDT	77.6	-2.65	3.95
	NET	22.4	-5.20	3.95
PFT-Adjusted Parameterization [PAP]	BDT	77.6	-3.24	2.93
	NET	22.4	-3.28	5.82
Species-Specific Parameterization [SSP]	Oak	15.2 [19.6]	-3.49	3.69
	Beech	62.4 [80.4]	-3.15	3.12
	Spruce	10.2	-3.5	3.69
	Douglas fir	12.2	-3.25	3.12

2.5 Numerical Experiments

Several numerical experiments were carried out by implementing standalone and mixed forests under different PHT parameterizations (Figure 2). In these experiments, the standalone forest parameterization is represented by an individual forest stand composed of only one PFT or species that covers 100% of the area and does not compete for water resources with other PFTs or tree species. In the mixed patched configuration, the forest is characterized by two or more forest types sharing the same lower boundary conditions (i.e., soil water resources). The fully-mixed configuration corresponds only to the broadleaf deciduous forest where Beech and Oak trees are randomly distributed. Different PHT parametrizations according to the forest stand classification (i.e., BDT, NET, Oak, Beech, Spruce, and Douglas fir) are used within each set of experiments. The basal area proportions of Oak and Beech were used to partition the observed leaf area index (LAI) at the site into species-specific LAI values in the model (see section 2.4.3).

Experiment 1 evaluates the difference in the forest response between standalone forest patches using GMP, PAP, and SSP PHT parameterization. This set of numerical experiments assesses the impact of using a different level of detail in the PHT parameterization; from biome-

generic PFT classification to species-specific hydraulic trait characterization. In this experiment the observed LAI of the site is assumed to represent only the proportion assigned to the one simulated PFT or species. Experiment 2 repeats the same assessment as Experiment 1, assuming a mixed patched forest where all patches share a common soil water store. In this second set of experiments the GMP and PAP parameterizations use the basal area proportion of NET and BDT in the catchment, which corresponds to 22.4% and 77.6%, respectively (Table 2). In the mixed patched forest configuration using the SSP parametrization, the area is subdivided according to the following percentages: Spruce (10.2%), Douglas fir (12.2%), Oak (15.2%), and Beech (62.4%). For Spruce and Douglas fir, these percentages were obtained from aerial photographs because these stands are established as mono-species plantations. The percentage of Oak and Beech was determined according to the proportion of the basal area contribution of each species (see Text S1), because these species grow in a mixed stand and their cover fractions cannot be easily distinguished in aerial photographs. Finally, Experiment 3 evaluates the effect of a fully-mixed forest stand that is represented only by the BDT in the catchment. This experiment considers the GMP and PAP PHT parameterizations of the BDT and the SSP of Oak and Beech. This forest stand comprises Beech (80.4%) and Oak (19.6%) trees, allowing us to compare the representation of a fully-mixed condition.

For each set of numerical experiments, we examined the impact of the different model parameterizations on the simulated transpiration and tree water stress as a consequence of plant hydraulic traits and competition for available water resources. This evaluation is carried out by separating normal and extremely hot years. We hypothesize that a higher level of PHTs refinement for the selected PFTs and tree species leads to a better agreement between simulated and measured signals of vegetation states (i.e., water stress) and fluxes (i.e., transpiration) than the generic PFT parameterization.

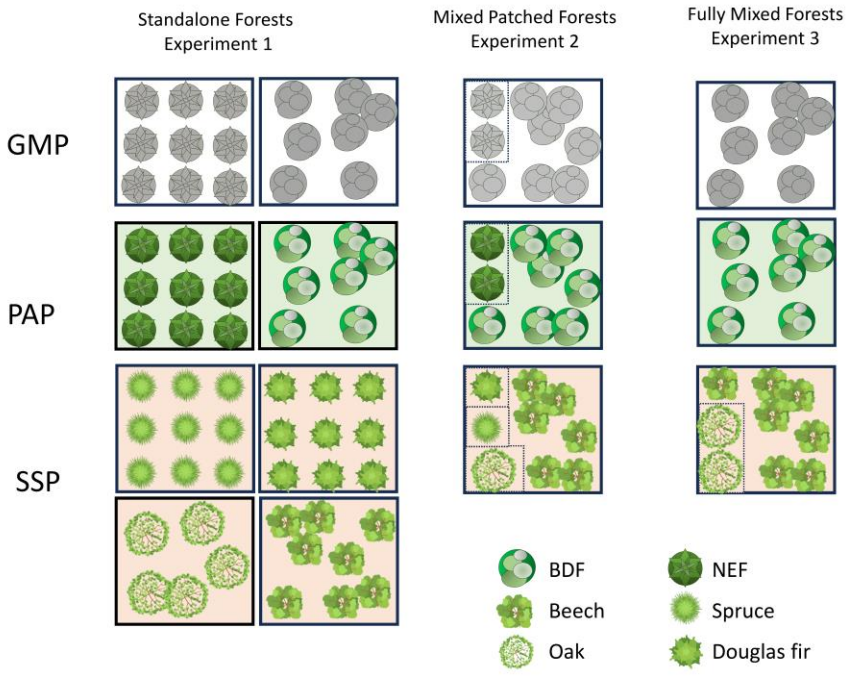

Figure 2. Schema of the three sets of numerical experiments carried out at the Weierbach catchment. A solid line frame represents the total ground area and a shared water resource, while

the dotted line frames represent the reference ground area for a given forest stand. Columns represent different experiments, rows different PHT parameterizations. GMP: generic model parameterization; PAP: PFT-adjusted parameterization; SSP: species-specific parameterization; BDF: broadleaf deciduous forest; NEF: needle-leaf evergreen forest. The tree crown images were retrieved from pch.vector (2023).

2.6 Data analysis

The data analysis was carried out for the extended summer period (i.e., May to September) due to the deciduous nature of the larger proportion of forest in the catchment (i.e., BDT). The analyses involving the measured tree transpiration ($E_{T\text{-}mea}$) are based on the years 2019 and 2020, while the evaluation of tree water deficit (TWD) is based on the years 2020 and 2021, because this is the only period in which all the species were simultaneously monitored. The classification of years into normal and hot is based on the total number of days classified as a heatwave for Luxembourg according to the European Drought Observatory (EDO, 2023). This classification uses the definition given by Lavaysse et al., (2018) who defined a heatwave as the period of at least three consecutive days with daily minimum and maximum air temperatures above the 90^{th} percentile of the baseline period. We used the same baseline period implemented by the EDO to determine the threshold between normal and hot years in Luxembourg (1980-2010). This threshold corresponds to the average plus one standard deviation (5.8 + 3.3 days), leaving a value of 10 days per year. Consequently, the years 2019 and 2020 were classified as hot years and 2021 as a normal year.

2.6.1 Principal Component Analysis

A principal component analysis (PCA) was carried out to evaluate the dependency of $E_{T\text{-}mea}$ and TWD on environmental factors. The environmental factors evaluated were air temperature (T), relative humidity (RH), incoming short-wave radiation (R_s), wind speed (u), and soil water content (θ). The meteorological variables used for the PCAs were extracted from the model atmospheric forcing (see section 2.4.1). The θ was measured at seven monitoring clusters established in the catchment (Hissler et al., 2021), obtaining the daily values by averaging soil moisture across depths (10 cm, 20 cm, 40 cm, and 60 cm) and monitoring clusters (see Figure S4).

2.6.2 Index of Agreement

Measured ($E_{T\text{-}mea}$) and modeled ($E_{T\text{-}mod}$) transpiration estimates were aggregated at the daily scale because sap flow does not translate directly to transpiration rates due to tree capacitance. These estimates were compared against each other using the index of agreement (I_{oa}) proposed by Duveiller et al., (2016). The I_{oa} (Equation 3) is the product of an α coefficient and the Pearson correlation coefficient (r). The α coefficient quantifies the bias existing between measured and modeled daily transpiration rates, where a value of 1.0 represents a perfect agreement between both data sets and a 0 value means no agreement between them. This coefficient is determined using the standard deviation of measured and modeled transpiration (σ_X and σ_Y, respectively) and their mean values ($\overline{X}$ and $\overline{Y}$). For the mixed forest conditions (i.e., Experiments 2 and 3) we discretize the I_{oa} between the different forest fractions ($I_{oa\text{-}F}$) to be compared with the I_{oa} at grid cell level ($I_{oa\text{-}G}$).

$I_{oa} = \alpha r$ where $\alpha = f(x) = \begin{cases} 0, & \text{if } r \leq 0 \\ \dfrac{2}{\frac{\sigma_X}{\sigma_Y} + \frac{\sigma_Y}{\sigma_X} + \frac{\left(\overline{X} - \overline{Y}\right)^2}{\sigma_X \sigma_Y}}, & \text{otherwise} \end{cases}$	Equation 3

2.6.3 Plant Water Stress Analysis

The model results include the estimations of water potential in roots (Ψ_{root}), stem (Ψ_{stem}) and leaf (Ψ_{leaf}). However, we selected only Ψ_{root} and Ψ_{leaf} to compare with the TWD considering the lack of differences between Ψ_{stem} and Ψ_{leaf} in the model results and the vulnerability segmentation hypothesis (Tyree & Ewers, 1991) which states that the distal portions of the plant (i.e., roots and leaf) are the most vulnerable sections of the plant. The tree water deficit (TWD) was correlated with the selected water potentials (i.e., (Ψ_{root} and Ψ_{leaf}) during the hot year and the normal year (i.e., 2020 and 2021, respectively). The Ψ_{root} corresponds to the integral of water potentials of all root segments along the soil profile. The Ψ_{leaf} is the weighted average of shaded and sunlit leaves according to their LAI values. The simulated matric potential data (i.e., Ψ_{root} and Ψ_{leaf}) and canopy stress factor (β) were averaged only for daytime conditions (i.e., from 06:00 to 18:00). The model uses Equation 4 to estimate the leaf water stress factor (β_x) as the ratio of the actual stomatal conductance ($g_{x.s}$) over the unstressed stomatal conductance ($g_{x.max}$) of each component of the canopy (i.e., sunlit and shaded leaf). Then, Equation 5 determines β as the weighted average of the canopy component and its corresponding LAI. The β ranges from 0 when the canopy is fully stressed to 1 when the canopy is unstressed. More details on the mathematical formulation of β in CLM5 are provided by Kennedy et al. (2019).

$\beta_x = \dfrac{g_{x.s}}{g_{x.max}}$	Equation 4

$\beta = \dfrac{\beta_{sunlit} \cdot LAI_{sunlit} + \beta_{shaded} \cdot LAI_{shaded}}{LAI_{sunlit} + LAI_{shaded}}$	Equation 5

2.6.4 Identification of stress periods based on the plant hydraulic system

We performed an additional assessment to test the feasibility of using the plant hydraulic system (PHS) of CLM5 to detect the historical stress periods linked to hot years according to the EDO classification at Weierbach. Here we referred to the mixed patched forest configuration used in Experiment 2 and adopted the plant specific hydraulic parameterization (see Section 2.5). We used the simulations of the 11-year time window (2011-2021), which contains four years classified as hot (i.e., 2015, 2018, 2019, and 2020) and the remaining seven years as normal years (see Section 2.6). Different physiological metrics extracted from the PHS of CLM5 namely β, Ψ_{root} and Ψ_{leaf}, were assessed as suitable indicators for detecting stressed forest ecosystems.

3 Results

3.1 Forest response to environmental conditions

In the Weierbach catchment, two key tree physiological variables, forest transpiration (E_T) and tree water deficit (TWD), were measured. Figure 3.A and Figure 3.B illustrate their primary differences on an annual basis, facilitating a comparison of transpiration responses and tree water status at different levels such as catchment, plant functional type (i.e., NET, BDT), and species (i.e., Spruce, Douglas fir, Oak, Beech). Figure 3.C and Figure 3.D present the outcomes of the principal component analysis (PCA), a crucial tool for identifying the main environmental variables influencing the variations in both E_T and TWD. The PCA analysis is pivotal in determining the most suitable indicators of tree physiological stress effects, which can then be utilized in the analysis of results obtained from numerical experiments.

The E_T estimates of all the forest stands were scaled up to the catchment area, revealing significant differences in contribution among various forest stands, such as Beech versus Oak, with minor interannual changes (Figure 3.A). The interquantile range of catchment-scale E_T (i.e., Wei. in Figure 3A) ranges between 0.5 mm d^{-1} and 3.0 mm d^{-1} for 2019 and 1.0 mm d^{-1} and 4.0 mm d^{-1} for 2020, reaching a maximum of 5.8 mm d^{-1} on certain days in June 2020 (see Figure S5). Segregation of E_T per plant functional type (PFT) indicates that broadleaf deciduous trees (DBT) contribute more significantly than needleleaf evergreen trees (NET). Among individual species, Beech stands out as the largest contributor to catchment E_T, reaching up to 3.0 mm d^{-1}, with peak rates during 2020. Oak transpiration is at most 1.0 mm d^{-1}, with its highest E_T occurring in 2019 (see Figure S5). In contrast, needleleaf trees (Douglas Fir and Spruce) exhibit similar transpiration rates between the two years, not exceeding 0.5 mm d^{-1} due to the smaller area they occupy in the catchment.

The PCA highlights that E_T of all forest stands is primarily influenced by solar radiation (R_s) and relative humidity (RH) (Figure 3.C). R_s lies parallel to the first dimension of the PCA, which explains more than 70% of the variability of the E_T and environmental variables (Figure 3.C). R_s has correlation coefficients larger than 0.8 with the E_T from all the forest stands (see Figure S6). Conversely, the RH is negatively correlated with E_T, showing values below -0.65. It is noteworthy that θ has on E_T for all the forest stands, with negative correlation coefficients close to -0.3, which are not statistically significant ($p > 0.05$). This indicates that the E_T response at the selected site, for all tree stands, is primarily an atmospheric-driven process.

In the hot year (2020), all species and PFTs experienced higher TWD compared to the normal year (2021) (Figure 3B). Notably, the distribution of TWD does not overlap between the two years for all forest stands, with only some outliers in the normal year reaching the median value of the hot year. At the PFT level, the bimodal distribution of TWD in Douglas fir during the hot year (2020) indicates a significant shrinkage of the monitored tree during the summer, followed by a sudden swelling process in autumn. Oak, Beech, and Douglas fir show a distinct breaking point where the TWD measurements do not overlap between years (except for outliers), with values of approximately 300 µm for Beech, 400 µm for Oak, and 100 µm for Douglas fir. In contrast, Spruce does not exhibit such a breaking point. The BDT displays the most significant differences between years, with the TWD values in the hot year being twice as high as those recorded during the normal year. At the species level, Oak and Beech trees show the most substantial differences, influencing the response of the entire BDT forest stand (Figure 3B). Among needleleaf trees, Douglas displays the largest variability in TWD between years, while

the differences for Spruce are less pronounced. The PCA of TWD indicates that variations are primarily explained and negatively correlated with θ (Figure 3D). Other environmental variables have a lower influence on the TWD response of the different forest stands (see Figure S7). The proximity of all forest stands in the PCA highlights a consistent pattern where TWD is dependent on changes in θ, making this measurement a robust indicator of the soil water stress experienced by forest ecosystems. However, it is less indicative of atmospheric water stress, as variables like R_s, u (wind speed), and T (air temperature) are orthogonal to the TWD of different species.

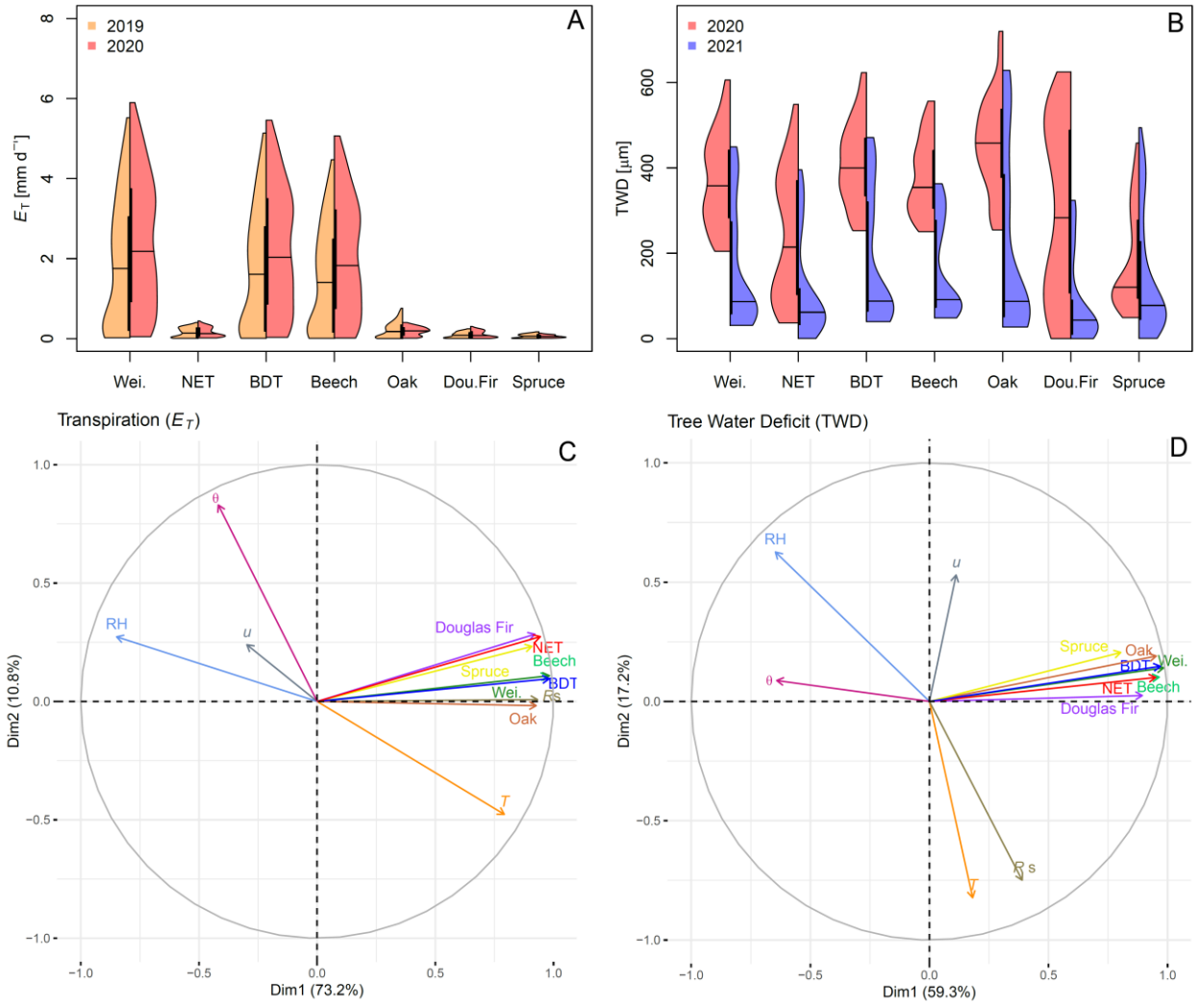

Figure 3. Summary of the observed forest response to environmental drivers. The upper plots (i.e., A and B) represent the interannual variability of transpiration (E_T) and tree water deficit (TWD), respectively. The lower plots (i.e., C and D) are the correlation circles of the principal component analysis (PCA). Each PCA shows the two main dimensions of the analysis that explain at least the 50% of all the data variability. The arrows labelled with species or PFT names represent either E_T (Panel C) or TWD (Panel D) for each species or PFT.

3.2 Standalone Forest Experiment

When examining each forest stand as an independent entity (Experiment 1), the E_T shows larger values across PHT parameterizations (i.e., GMP, PAP, SSP) when the canopy stress factor (β) ranges between 0.6 and 0.8. The results highlight the absence of periods with a stressed canopy (β<0.5). Among the needleleaf forest stands, NET-GMP exhibits the lowest index of agreement (I_{oa}) between simulated E_T and observed sap flux (I_{oa}: 0.48), indicating a consistent overestimation of E_T throughout the growing season (see Figure S8). The performance of the NET standalone parameterization significantly improves when using the PAP parameterization, with I_{oa} increasing to 0.75. This improvement reduces the E_T bias throughout 2019, yet the overestimation persists during the second half of the growing season of 2020 (see Figure S8). Conversely, employing a SSP PHT parameterization for needleleaf species leads to a marginal and minor improvement on the I_{oa} compared to the GMP parameterization for Douglas fir (I_{oa}: 0.563) and Spruce (I_{oa}: 0.692), respectively. The PHT parameterization of Douglas fir maintains a low bias in 2019 but struggles to reproduce E_T in 2020, resulting in a large bias (see Figure S8). Transitioning from GMP to PAP in the BDT PHT parameterization has a negligible effect on I_{oa}, increasing from 0.757 (GMP) to 0.774 (PAP). However, both GMP and PAP parameterizations systematically underestimate E_T for both years (2019 and 2020). With the implementation of the SSP parameterization, the performance of the individual BDT forest stands deteriorates in both years (see Figure S8) compared to the GMP and PAP parameterizations. The SSP for Oak mostly underestimates E_T, with a mean absolute error of 0.9 mm d^{-1}, while SSP-Beech underestimates E_T with a mean absolute error of up to 1.8 mm d^{-1}, resulting in low I_{oa} values of 0.58 and 0.55, respectively (see Figure S8).

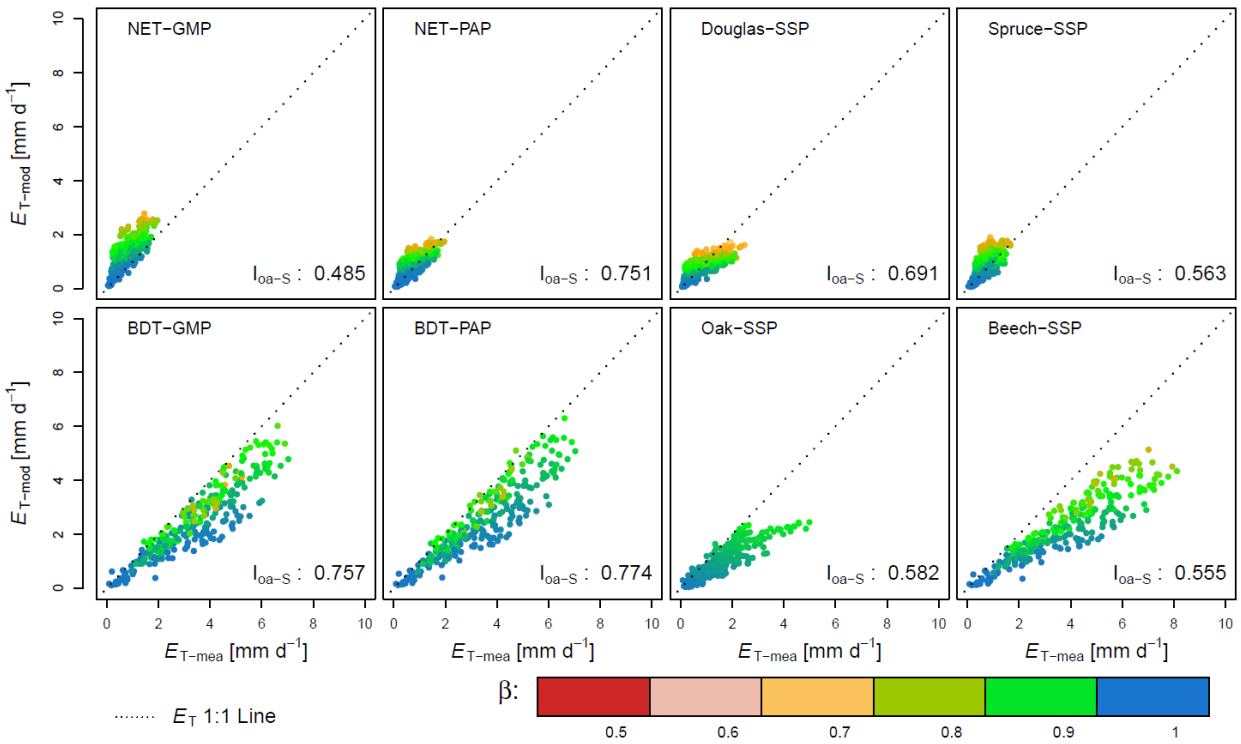

Figure 4. Modeled ($E_{T\text{-mod}}$) and measured transpiration rates ($E_{T\text{-mea}}$) of the standalone forest stands using the generic model parameterization (GMP), the PFT-adjusted parameterization (PAP), and the species-specific parameterization (SSP). The canopy stress factor (β) is used to visually characterize stress at the leaf level.

The simulated Ψ_{root} values for all PHT parametrizations of NET remain unchanged between the hot year (2020) and the normal year (2021). These Ψ_{root} values exhibit a negative correlation with TWD, indicating that more negative Ψ_{root} values are associated with higher TWD (Figure 5). This negative correlation is statistically significant only for the GMP parameterization. It is worth mentioning that the lower Ψ_{root} values produced by the GMP parameterization result from the associated Ψ_{p50} parameter that is almost 2.0 MPa lower than that of the PAP and SSP parameterizations (Table 2). It's important to highlight a notable difference in the relationship between the simulated Ψ_{root} and measured TWD between the hot and normal years for BDT species. In 2020, all three parameterizations (GMP, PAP, SSP) show a significant negative correlation between TWD and Ψ_{root}, with a p-value less than 0.001. However, in 2021, they are uncorrelated. Finally, it is interesting to highlight the different ranges of water potential values simulated for the roots of NET and BDT trees, driven by the different Ψ_{p50} values as defined by the PHT parameterization (Table 2).

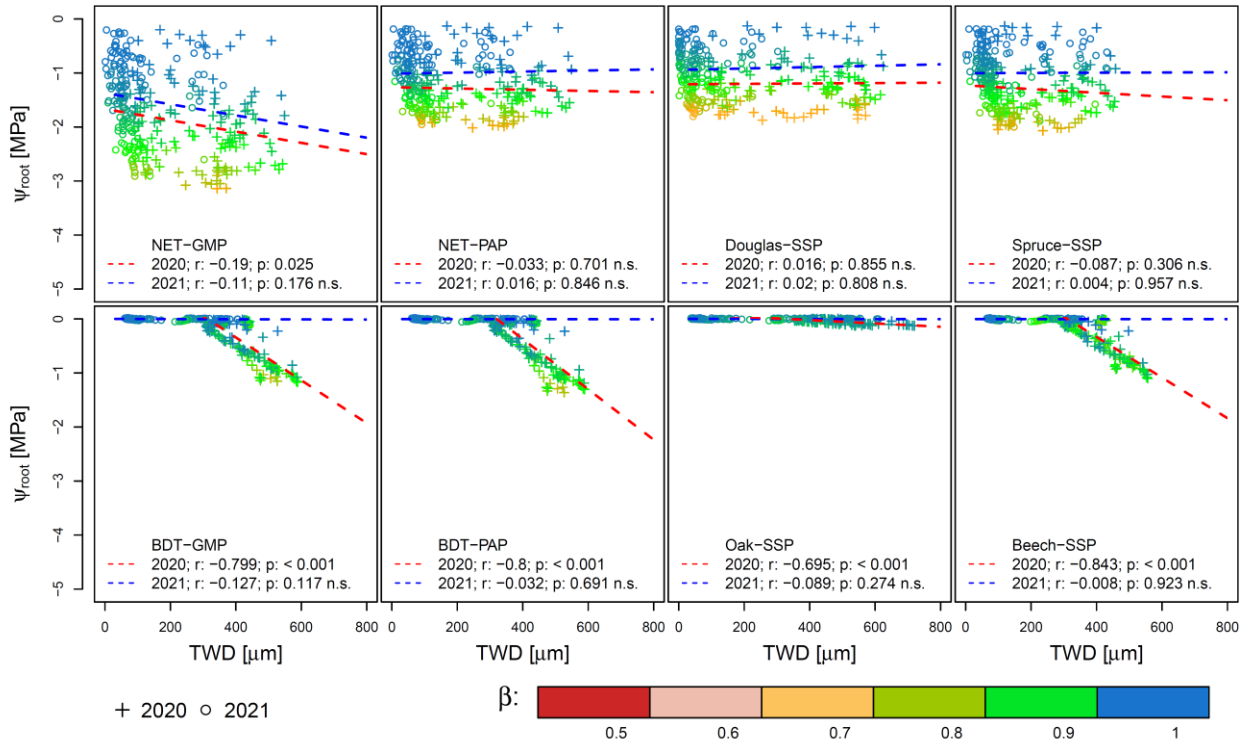

Figure 5. Correlation between simulated root water potentials (Ψ_{root}) and measured tree water deficit (TWD) of the standalone forest stands (Experiment 1) using the generic model parameterization (GMP), PFT adjusted parameterization (PAP), and Species-Specific Parameterization (SSP). The canopy stress factor (β) is used to visually characterize the stress at leaf level. The p-values (p) of the Pearson correlation coefficient (r) are not significant when marked with n.s.

3.3 Mixed Patched Forest experiment

The three PHT parameterizations exhibit minimal differences in E_T magnitude and canopy stress (β). These minor differences are reflected in the values of the index of agreement (I_{oa}), ranging from 0.798 (SSP PHT) to 0.824 (GMP PHT). Despite these nuances, the relationship between Ψ_{root} and TWD is not significant in 2021 for all model parameterizations (i.e., GMP, PAP, and SSP). However, a significant ($p < 0.001$) and negative correlation is observed for 2020 (Figure 6). It's noteworthy to highlight the remarkably similar range of Ψ_{root} values (0 - 1.5 MPa) simulated by the model despite the distinct Ψ_{p50} values used by NET (i.e., -5.2 MPa) and BDT (i.e., -2.65 MPa) in the GMP parameterization. This suggests that BDT forest types play a crucial role as the main driver of the ecosystem status at the grid cell level.

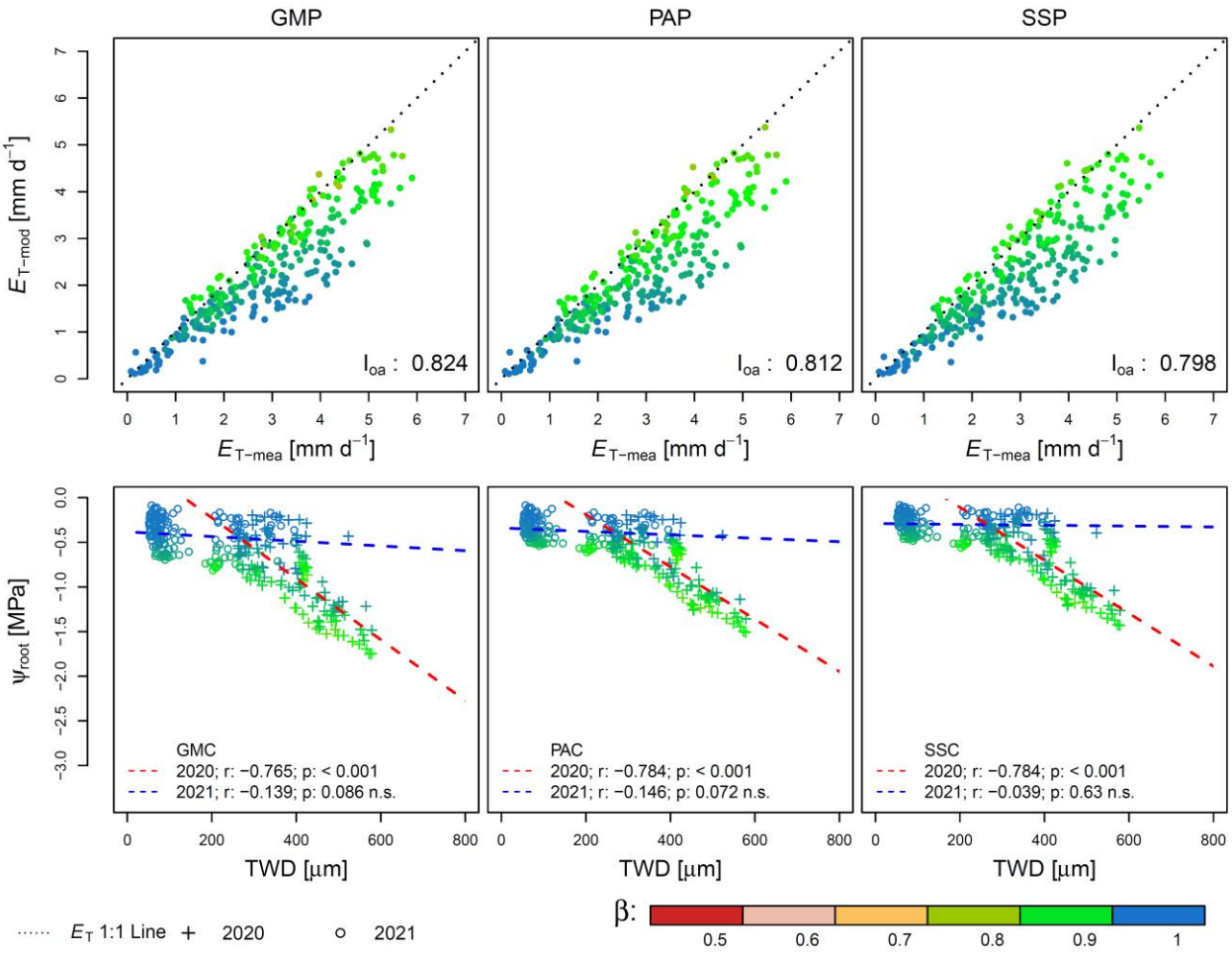

Figure 6. modeled (E_{T-mod}) and measured (E_{T-mea}) transpiration and the correlation between root matric potentials (Ψ_{root}) and tree water deficit (TWD) of a mixed patched forest (Experiment 2) using the generic model parameterization (GMP), the PFT adjusted parameterization (PAP), and the Species-Specific Parameterization (SSP). The canopy stress factor (β) is used to visually characterize the stress at the leaf level of each parameterization. The p-values of the Pearson correlation coefficient (r) are not significant when marked with n.s.

The performance of the simulated E_T of the individual fractions of the mixed-patched forest under all three parameterizations (i.e., GMP, PAP, SSP) is illustrated in Figure 7. It is crucial to emphasize that differences in E_T between the fractions arise from their proportional contribution to the overall forest composition. Additionally, the sum of the individual contributions always equals the grid cell values (grey background dots in each subplot). The simulated E_T values are associated, even in this experiment, with mild canopy stress conditions, reflected by β values ranging between 0.7 and 0.8.

For the NET forest fraction, both GMP and PAP parameterizations tend to overestimate E_T. However, the level of agreement (i.e., I_{oa}) between modelled and measured transpiration values improved significantly (from 0.517 to 0.763) when the PHT parameterization at the PFT level is refined. In contrast, the modeled E_T for the BDT fraction underestimates the actual E_T, with negligible differences between the GMP and PAP parameterization. However, when the

SSP parameterization is applied in the mixed-patched forest configuration, the results for NET and BDT species are remarkably different. NET species reach an I_{oa} of 0.723 and 0.616 for Douglas fir and Spruce, respectively, while BDT species have values of 0.656 and 0.672 for Oak and Beech, respectively. The low performance of BDT species is due to an overestimation of ~50% for Oak and an underestimation of one-third for Beech compared to measured E_T. Refining the PHT parameterization does not substantially affect the performance of the model when analyzing its integrated response at the grid cell level ($I_{oa\text{-}G}$ values range between 0.79 and 0.82). However, it has significant implications in the analysis of the transpiration response of individual fractions. The use of a refined PHT plays an important role in improving the simulated model response for those needleleaf evergreen species growing as isolated patches within the catchment. Conversely, the improved PHT parameterization does not enhance the simulation of the transpiration response for those broadleaf species growing in fully-mixed forest stands. Interestingly, there is an increment in I_{oa} when moving from standalone conditions (Experiment 1) to mixed patched forest conditions (Experiment 2) for all species. The improvement in I_{oa} for Douglas fir (from 0.692 to 0.723) is slightly lower compared to that of Spruce (from 0.563 to 0.616), Oak (from 0.58 to 0.66), and Beech (from 0.55 to 0.67).

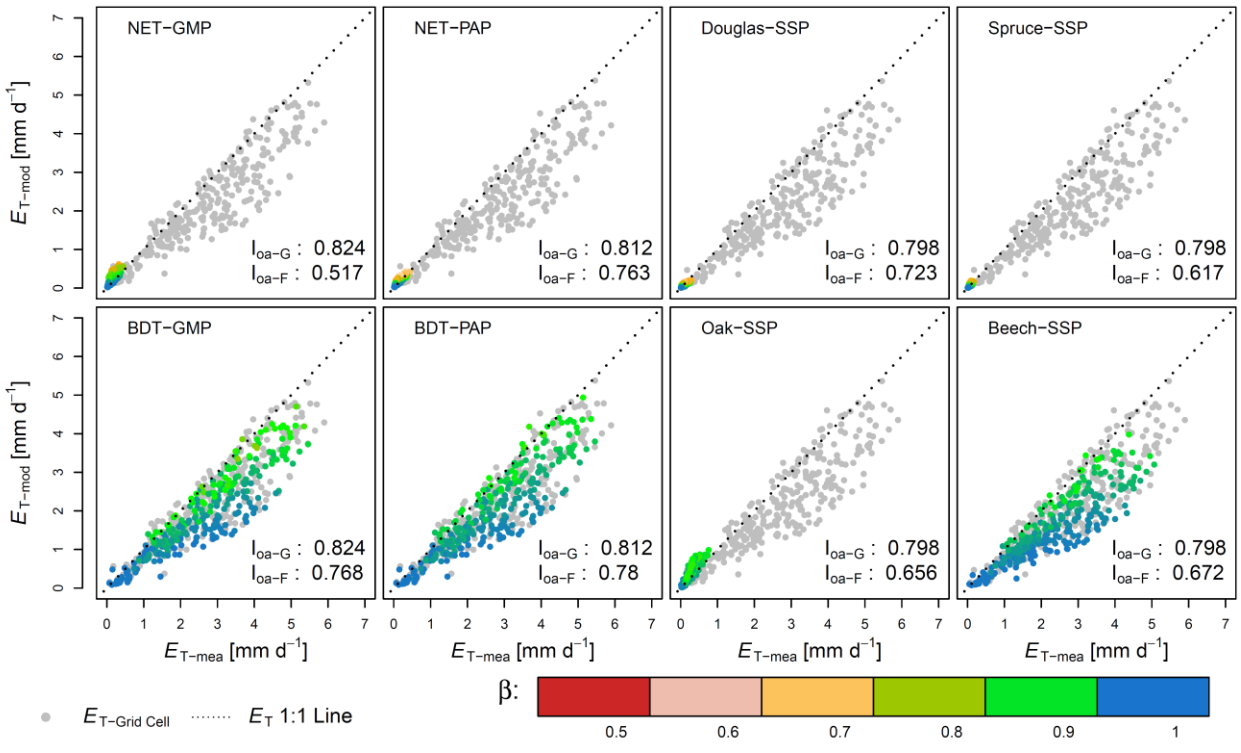

Figure 7. Simulated ($E_{T\text{-}mod}$) and measured ($E_{T\text{-}mea}$) transpiration rates of the individual fractions of a mixed patched forest (Experiment 2) using the generic model parameterization (GMP), the PFT-adjusted parameterization (PAP), and Species-Specific Parameterization (SSP). The canopy stress factor (β) is used to visually characterize the stress at the leaf level of each parameterization. The grey dots represent the $E_{T\text{-}mod}$ of the grid cell for each PHT parameterization according to the results in Figure 6. Each plot has two indices of agreement representing the grid cell ($I_{oa\text{-}G}$) and the individual fractions within the grid cell ($I_{oa\text{-}F}$).

Figure 8 illustrates the relationship between the Ψ_{root} and TWD for the mixed patched forest condition (Experiment 2). In this model configuraiton, there is a significant negative correlation ($p<0.001$) between these two variables for both BDT and NET PFTs during the hot year (i.e., 2020). This significant relationship persists across PHT parameterizations for both PFTs. A clearer signal is obtained when using the SSP parameters for both Oak and Beech in the case of BDT and for Spruce in the case of NET. Note that this significant relationship did not emerge for NET in Experiment 1 when this ecosystem was simulated as a standalone forest stand. Similarly, the relationship between Ψ_{root} and TWD for BDT differs between Experiment 1 and Experiment 2. In mixed-patched conditions, trees share the same soil water resources, the signal emerging for Oak species is highly influenced by Beech species due to their larger water use that drives the soil water changes in the catchment. Lastly, it is interesting to highlight that Ψ_{root} remained close to zero in the wetter year (i.e., 2021) and when TWD is less than 300-400 µm during the hot year (i.e., 2020). However, when TWD exceeds 300-400 µm in the hot year, there is a significant negative correlation between Ψ_{root} and observed TWD.

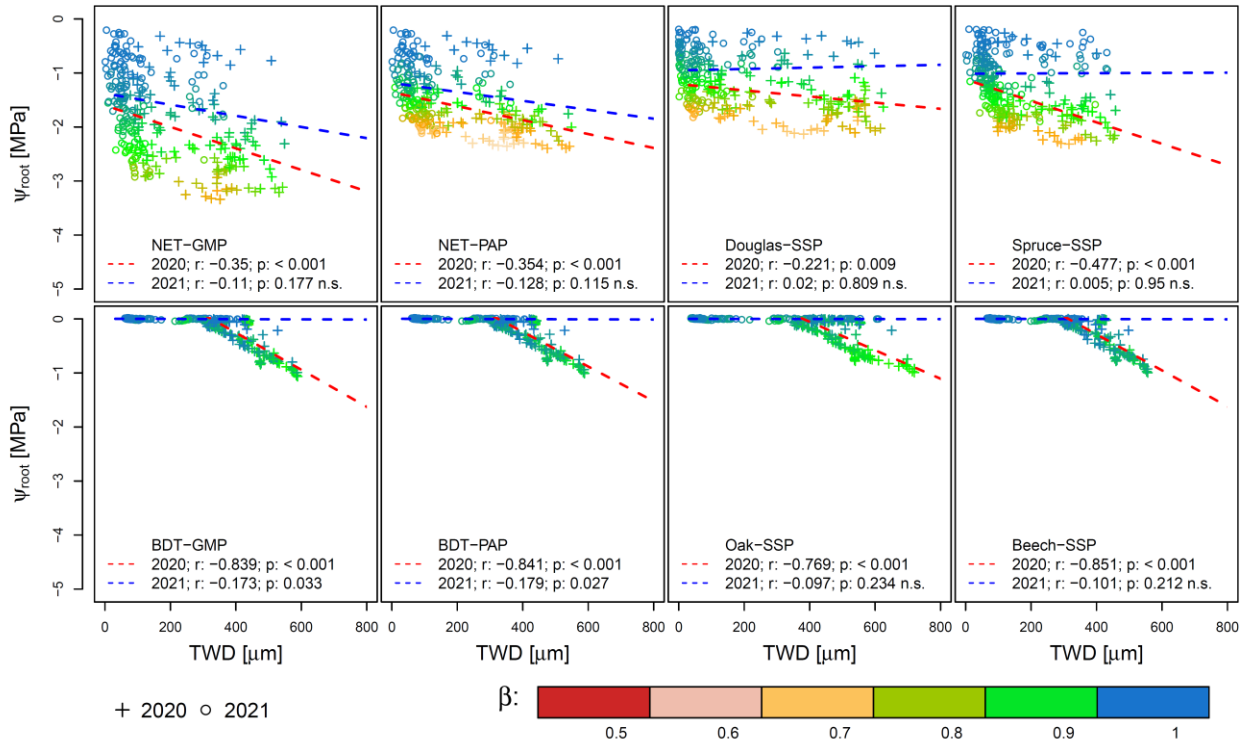

Figure 8. Correlation between the root matric potentials (Ψ_{root}) and tree water deficit (TWD) of the mixed patched forest (Experiment 2) using the generic model parameterization (GMP), PFT adjusted parameterization (PAP), and Species-Specific Parameterization (SSP). The canopy stress factor (β) is used to visually characterize stress at the leaf level. The p-values of the Pearson correlation coefficient (r) are not significant when marked with n.s.

3.4 Fully-mixed Forest Experiment

Figure 9 compares the results of Experiment 3, where fully-mixed conditions are represented only by the BDT PFT at the Weierbach catchment. The I_{oa} values of the three PHT parameterizations (i.e., GMP, PAP, SSP) do not differ substantially at the grid cell level, with a minor increase from 0.757 to 0.778 when moving from GMP to SSP (see Figure S2 and Table 2). The SSP parameterization enhances modeled E_T for individual species when compared with the standalone condition of Experiment 1. The I_{oa} increases for both Oak (from 0.582 to 0.674) and Beech (from 0.555 to 0.664). The shared resources at the grid cell (i.e., the soil compartment) and a similar PHT influence the strong similarities in Ψ_{root} among parameterizations, where the GMP shows a slight difference with PAP and SSP at the grid cell level. The differentiation between the hot year (2020) and normal year (2021) year follows the same trend as in Experiment 1 for GMP-BDT, PAP-BDT, and SSP-Beech. However, when Oak shares the soil water resources with Beech (i.e., Experiments 2 and 3), the Oak fraction depicts more negative Ψ_{root} than in Experiment 1.

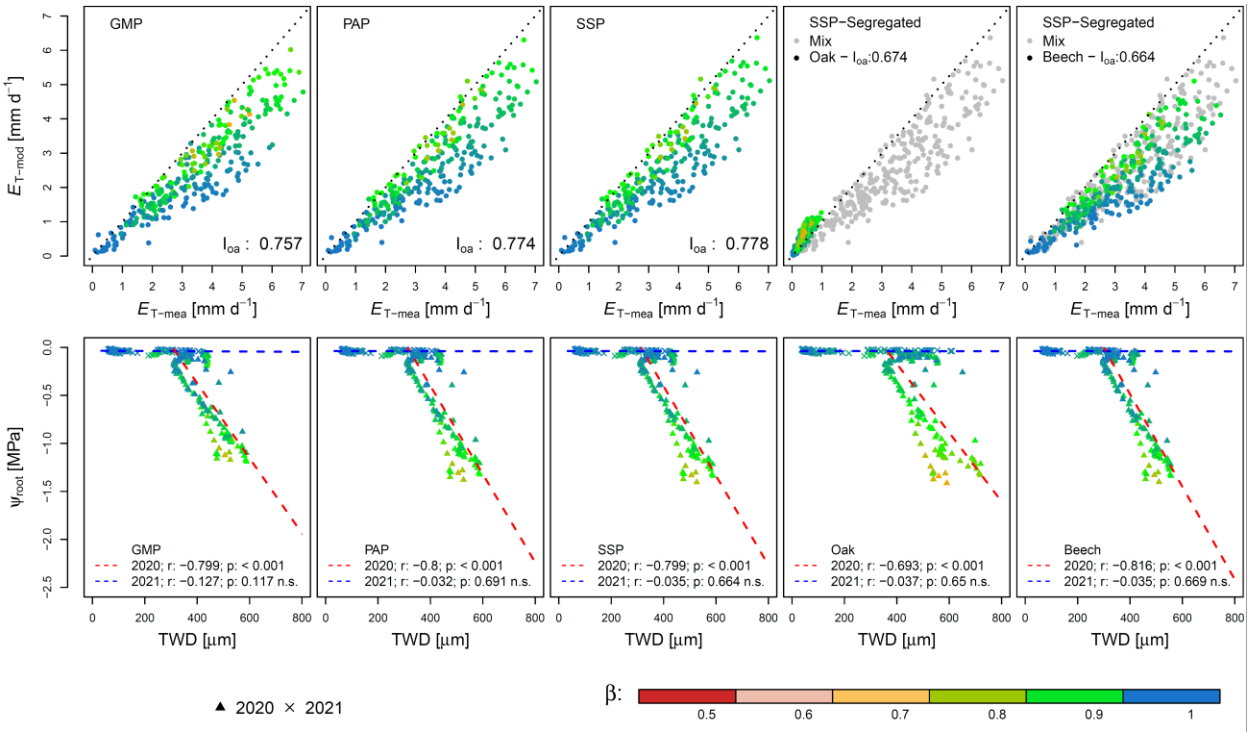

Figure 9. Modeled ($E_{T\text{-}mod}$) and measured ($E_{T\text{-}mea}$) transpiration and the correlation between the root matric potentials (Ψ_{root}) and tree water deficit (TWD) of a fully-mixed forest (Experiment 3)

using the generic model parameterization (GMP), the PFT-adjusted parameterization (PAP), and the Species-Specific Parameterization (SSP). The canopy stress factor (β) is used to visually characterize stress at the leaf level of each parameterization. The p-values of the Pearson correlation coefficient (r) are not significant when marked with n.s.

3.5 Identifying the stress periods at Weierbach

In the 11-years of simulations, the mean daily air temperatures of the four hot years (i.e., 2015, 2018, 2019, 2020) exceeded 27 °C for prolonged periods in spring and summer, with big differences in frequency and timing among the years (see Figure S12). The response of the canopy stress factor (β) and leaf water potential (Ψ_{leaf}) to high air temperatures is similar between normal and hot years, hampering a characterization of the stress periods based on these metrics. Conversely, the root water potential (Ψ_{root}) provides a good differentiation between hot and normal years for broadleaf (i.e., BDT, Oak, Beech) forest fractions, but not for the needleleaf (i.e., NET, Douglas fir, Spruce) forest fractions (Figure 10). This contrast showed by broadleaf and needleleaf forest fractions for the Ψ_{root} is diluted at grid cell level, where the differentiation between normal and hot years shows a mixed response from both land covers (see Figure S14). By selecting the minimum Ψ_{root} value (1st quantile) of normal years as an assumed limit for stress conditions (dotted blue line in Figures 10 and S14), it is possible to identify the periods were the vegetation experiences more stress in broadleaf forest and at grid cell level but not for the needleleaf forest.

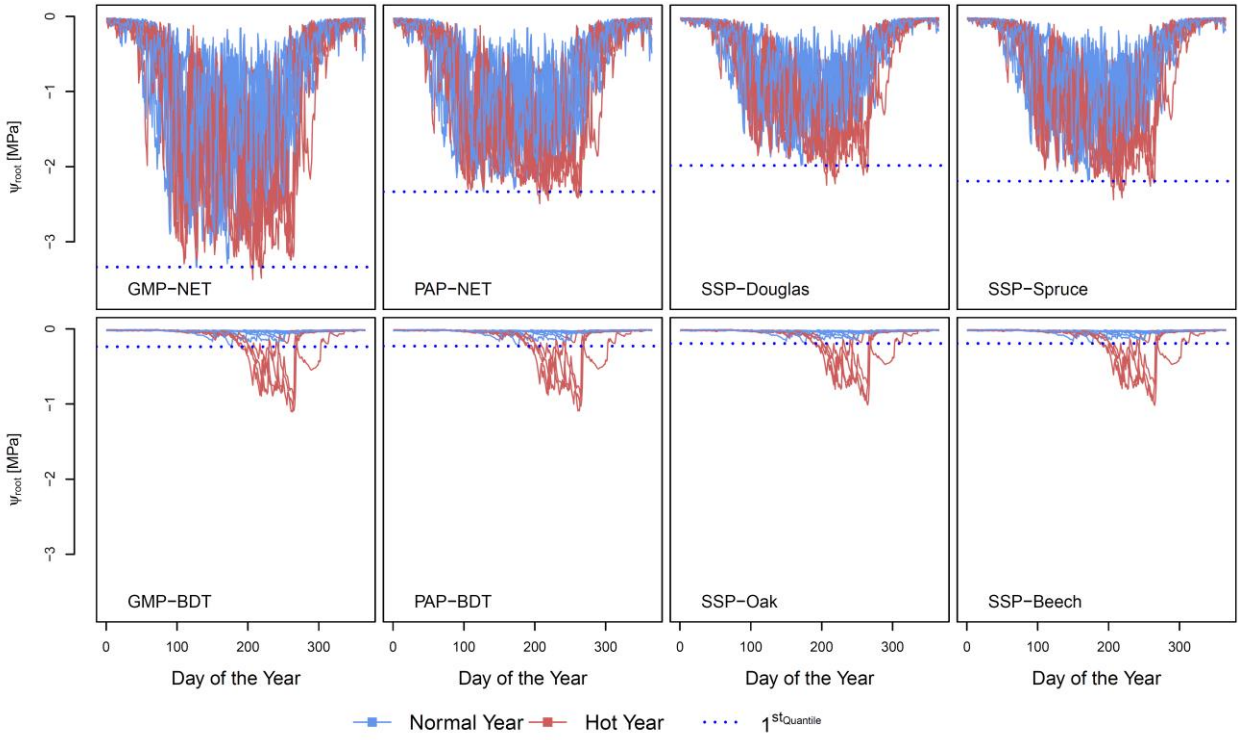

Figure 10. Multiannual variability of the root (Ψ_{root}) water potentials per forest fraction simulated for the period between 2011 and 2021 at the Weierbach catchment. The distinction between normal and hot years is made according to the European Drought Observatory (EDO, 2023) classification and based on the meteorological observations in Luxembourg. Each line

corresponds to an individual year modeled between 2011 and 2021, differentiated between normal (blue lines) and hot (red lines) years.

4 Discussion

4.1 Importance of a refined plant hydraulic representation of mixed forests

The data from experimental forest stands are crucial in benchmarking physiological processes in vegetation (e.g., Chaney et al., 2016; Sabot et al., 2020). Most datasets describing PHTs are based on forest stands of different ages, management practices, and plant organs (e.g., Choat et al., 2012), so caution is advised when using them widely to describe vegetation (Chu et al., 2021). The characterization of PHTs per individual PFT lumps species together by considering only the latitude and plant physiognomy (e.g., Lin et al., 2015), neglecting regional and current distribution of tree species. Physiological characterization is fundamental to reproducing vegetation water use strategies in CLM5 (Vidale et al., 2021). Li et al. (2021) stressed the importance of implementing a better hydraulic trait-based representation to improve the flux simulations in land surface models (LSMs) during drought events. This is crucial because CLM5's generic parameterization is highly sensitive to dry conditions, affecting gross primary productivity (GPP) and E_T fluxes (e.g., Jiménez-Rodríguez et al., 2022; Wu et al., 2020).

While some assume that CLM5's PHT parameterization represents ecosystems correctly (e.g., Raczka et al., 2021; Wu et al., 2020), present study shows differences in PHT leading to an overestimation of E_T in the GMP compared to PAP or the SSP. Some have improved the PHT parameterization of CLM5, enhancing the representation of the tree species in several forest stands dominated by a single tree species (e.g., Ali et al., 2022; Jiménez-Rodríguez et al., 2024). In the present study, refining PHT parameterization for the individual needleleaf species (i.e., SSP-Spruce, SSP-Douglas fir) drastically improved modeled E_T. However, uncertainties in PHT for individual tree species complicate parameter selection, even at the species level (e.g., Lobo et al., 2018; Rosner et al., 2019). Refinement efforts for two broadleaf species (Oak and Beech) did not improve simulated E_T when considered as standalone forest patches, possibly due to different age structures and age-dependent PHT parameters (Lutz et al., 2013; Zeller & Pretzsch, 2019). Hence, by including the SSP we largely improved the E_T simulations of individual forest stands despite the small differences at grid cell level. This condition enforces the need for an individual evaluation of model performances for each forest fraction (Figure 7), rather than relying solely on aggregated values at the grid cell level (Figures 6).

To date, few studies have investigated the effect of refining the PHTs in CLM5 for fully-mixed forests. For example, Birch et al. (2021) and Kennedy et al. (2019), addressed the PHT characterization from a lumped perspective focusing on the overall fluxes (e.g., eddy-covariance data) and not on the individual performance at the species level. In the current study, LAI was segregated between Oak and Beech in a fully-mixed stand, and simulated E_T for both species was compared to sap flow data separated by species. Surprisingly, no improvement in E_T simulations resulted from species-specific PHT parameterization. This suggests potential deficiencies in other aspects of the model, such as the representation of water use strategies (Jiménez-Rodríguez et al., 2024), or competition for light and water resources between the species.

4.2 The stressed vegetation and the hidden roots

Extreme temperatures and drier soil conditions are the main factors causing a decline in gross primary productivity in forest ecosystems (J. Li et al., 2023). These conditions bring about significant changes in water potentials within the plant, helping identify periods of high stress when vegetation could suffer irreversible damage. Predawn water potentials ($\Psi_{predawn}$) have been used in the past to assess stress in forest ecosystems (e.g., Lavoir et al., 2009; Peiffer et al., 2014), even though continuous monitoring of $\Psi_{predawn}$ is challenging. Although there are no direct measurements of plant water potentials in the Weierbach catchment, insights into tree water status can be deduced from TWD, strongly linked to midday canopy water potentials (Steppe, 2018). Our PCA analysis shows that TWD measurements at Weierbach heavily depend on soil water content (θ), while remaining unaffected by atmospheric drivers (Figure 3D). Tree water storage has been identified as an effective mechanism that prevents trees from dehydrating when the air around them becomes dry (Preisler et al., 2022). The capacity of trees to store water depends on θ and their sapwood area (Hartzell et al., 2017). This helps them avoid stress caused by water shortage if the water supply is enough to meet atmospheric dryness. Trees in Weierbach have a considerably large sapwood area (see Table S3), which helps them buffer against atmospheric drought through their water storage capacity. This also strengthens the relationship between changes in θ and stem diameter (i.e., TWD).

The simulated root water potentials (Ψ_{root}) for all mixed forest configurations at the grid cell level and for all broadleaf parameterizations (i.e. BDT, SSP-Oak and SSP-Beech) show a strong negative correlation with observed TWD in the hot year, which is not observed in the normal year (Figures 5, 6, 8 and 9). In contrast, simulated leaf water potentials (Ψ_{leaf}) and Ψ_{root} for needleleaf species in the standalone simulations (Figure 5) are very noisy and do not show a clear difference between the years. However, when the needleleaf fractions are in a mixed forest configuration, their Ψ_{root} values do show a significant negative correlation with TWD (Figure 8), likely because of the strong influence of the co-occurring broadleaf species on the soil water resources. Considering that the measured TWD does reach higher values in the hot year compared to the normal year for all species and the expected link between TWD and canopy water potentials (Steppe, 2018), a stronger correlation between simulated water potentials and TWD could suggest a more realistic model simulation. Since the needleleaf species cover a separate part of the catchment in the Weierbach, it was not expected that they really do compete for water with the broadleaf species. However, the standalone model configuration resulted in worse reproduction of observed sap flux for the needleleaf trees (Figure 4 vs. Figure 7) and a lower correlation between TWD and Ψ_{root} than the mixed patched forest configuration (Figure 5 vs. Figure 8), suggesting that the latter configuration produced more realistic results.

When modeling mixed forest ecosystems, CLM5 uses a single lower boundary condition shared by multiple PFTs in each grid cell (Lawrence et al., 2019). This forces all PFTs to share the same soil moisture pool, meaning that the dominant PFT drives the transpiration response and water potentials of the other PFTs in a mixed forest configuration. The plant water uptake module allows the vegetation to use deeper water sources when the upper layers are too dry to supply the canopy water demand (Kennedy et al., 2019; Lawrence et al., 2019). This characteristic enables representation of the adaptability of adult Beech trees (Brinkmann et al., 2019) and deep water use by Oaks (Aranda et al., 2005; Bréda et al., 1993). However, it also allows species that usually rely on shallower soil water to use deeper resources, forcing an unrealistic response, as in the case of Spruce and Douglas Fir in Weierbach, where the vegetation

appears to be unaffected by water stress in the model. Therefore, when multiple PFTs share the same grid cell in CLM5, the dominant cover in the landscape will mask or dilute important aspects related to the water use of the other PFTs. This is the case in the Weierbach catchment, where BDT (for GMC and PAC) and Beech (for SSP) are the dominant forest fractions driving the E_T and hydraulic stress at the grid-cell level. The simplicity of the exponential root density profile used in most LSMs (e.g., JULES, CLM, ORCHIDEE) (Druel et al., 2017; Harper et al., 2021; Lawrence et al., 2019) does not represent recent evidence of rooting strategies where the fractional root allocation depends on the accessibility (e.g., depth) of the groundwater and capillary fringe by the vegetation (Perona et al., 2022; Wang et al., 2018) . Further, the exponential root profile used in LSMs overlooks the fact that vertical root distributions can be quite variable and dynamically follow changes in water availability (Fukuzawa et al., 2007; López et al., 2001; Zwetsloot & Bauerle, 2021).

4.3 The challenge of representing mixed forest ecosystems

The representation of PFTs in mixed forests is critical in LSMs because it may introduce significant uncertainties concerning carbon, energy, and water fluxes (Hartley et al., 2017). In CLM5, applying it to complex ecosystems can lead to biases in flux and water stress estimation (e.g., Song et al., 2020). Challenges arise in representing mixed patches and fully-mixed forests, depending on the spatial distribution and contribution of different tree species. In this context, patched mixed forests composed of well-spaced fractions that do not strongly interact hydrologically can easily be represented by separate grid cells due to their physiognomic differences (e.g., needleleaf versus broadleaf). In fully-mixed forest ecosystems (Experiment 3), where different tree species coexist and share soil resources, the random spatial distribution challenges accurate representation of individual species in the model, impacting the precise calculation of transpiration fluxes (e.g., E_T). This might explain why a more detailed characterization of PHT per species did not enhance E_T estimates (see Section 3.4). In the Weierbach catchment, the heterogeneous distribution of Beech and Oak trees leads to varied LAI per species across the landscape, influencing how the ecosystem responds to water-limited conditions (Forrester et al., 2022). The interactions among tree species and environmental drivers may induce the trees to express different PHT within the range of each species (Drew et al., 2011; Lobo et al., 2018). For example, it has been found that some vulnerable tree species are more resilient to drought conditions growing in a mixed forest stand than as a mono-specific stands (Schäfer et al., 2019).

4.4 Challenges and opportunities in identifying vegetation stress in land surface models

In previous CLM versions, vegetation stress metrics were tied to a soil stress factor (β_{soil}), connecting the soil compartment directly to the photosynthetic apparatus (Shrestha et al., 2018). CLM5 replaced this with the plant hydraulic system (PHS), using the plant vulnerability curve (PVC) for water transport and a canopy stress factor (β) for leaf-level gas exchange (Kennedy et al., 2019; Lawrence et al., 2019). However, using β alone as an indicator of tree stress in the Weierbach catchment is misleading (see Figure S13), as it does not capture the hydraulic stress conditions experienced by the species during the study period. To accurately identify stress periods in CLM5, it is necessary to go beyond β and consider other metrics. The static parameterization of PHTs in CLM5 ignores the temporal changes in plant physiology (Wieder et al., 2019), allowing the vegetation to fully recover after a stress period without accounting for its

duration. This contrasts with evidence suggesting slow recovery after extreme hydraulic stress in vegetation responses (Brodersen et al., 2019; Klein et al., 2018; Meinzer & McCulloh, 2013).

Using tree water deficit (TWD) as a proxy for canopy water potentials (Dietrich et al., 2018; Schäfer et al., 2019) suggests the possibility of using this variable as an indicator of stress. In the Weierbach catchment, TWD clearly indicates the periods when most tree species (i.e., Oak, Beech, and Dougas fir) are affected by hydraulic stress due to stem shrinkage. This stress is reflected in the model by the root water potential (Ψ_{root}) at the grid cell level, particularly for broadleaf covers, where Ψ_{root} is directly linked to soil water potential (Ψ_{soil}), driving the root system's response. The Weierbach catchment has experienced three consecutive hot years from 2018 to 2020 with limited water input. These frequent extreme weather events are likely to affect the vegetation's response to hydraulic stress, resulting in legacy effects. However, it's difficult to differentiate between normal and hot years using Ψ_{leaf} and β when compared to TWD. This could be due to the model's PHS not accounting for tree capacitance, leading to an unintended lack of legacy effects. The PHS includes the changes in θ as the drivers of legacy effects, which better represents the hydraulic stress response shown by TWD in Weierbach since the root system depends on Ψ_{soil}.

5 Conclusions

The forest's response to extreme weather events such as heatwaves is highly dependent on forest structure and species composition, where mixed forests are presumed to be more resilient to droughts. However, the representation of mixed forests using the plant functional type (PFT) classification system can misrepresent the stress response of such complex ecosystems. This work addressed these relevant scientific issues by implementing the Community Land Model version 5.0, at the experimental Weierbach catchment in Luxembourg. Several numerical experiments were carried out, assuming three forest conditions (i.e., standalone, mixed-patched, and fully-mixed forests). For each set of experiments, different plant hydraulic parameterizations were used to characterize the PHS of the model.

The forest transpiration (E_T) based on sap flow measurements did not exceed 4.0 mm d^{-1}, with minor differences between normal and hot years. Catchment E_T was strongly influence by solar radiation (R_s) and relative humidity (RH). The estimations of tree water deficit (TWD) based on incremental stem diameter recordings showed a strong difference between years, with the hot year (i.e., 2020) having much larger values than the normal year (i.e., 2021) across species and PFTs. The interannual differences of TWD were primarily affected by the soil water content (θ) suggesting that soil drought rather than atmospheric drought was the primary driver for vegetation stress.

The three numerical experiments showed that the characterization of plant hydraulic traits (PHTs) based on species rather than a "PFT-typical" parameterization improved the E_T estimates of homogeneous forest stands and to a lesser extent that of mixed forests. Also, the use of a refined parameterization improved the capability of the model in reproducing the vegetation water stress at both coarse (i.e., PFT) and fine (i.e., species) levels for the broadleaf stands. Representing fully-mixed forests as individual species showed limitations on the E_T estimates as even though the grid-cell level do not differ among parameterizations. These results highlight the importance of refining the characterization of the PHT assigned to conventional PFT, where the improvement should consider the spatial distribution of the species present in a region. The results of the numerical experiments showed the constraints to use the simulated root water

potential (Ψ_{root}) to identify hydraulic stress periods in needleleaf covers. Whereas the performance of Ψ_{root} in broadleaf covers highlighted its utility to identify such periods of hydraulic stress.

Acronyms

Acronym	Meaning
BDF	Broadleaf deciduous forest
BDT	Broadleaf deciduous temperate trees
EDO	European drought observatory
GMP	Generic model parameterization
LAI	Leaf area index
PAP	PFT adjusted parameterization
PCA	Principal component cnalysis
PFT	Plant functional type
Ioa	Index of agreement
	-f forest fraction
	-g grid cell level
NEF	Needleleaf evergreen forest
NET	Needleleaf evergreen temperate trees
PHS	Plant hydraulic system
PHT	Plant hydraulic traits
PLC	% loss of hydraulic conductance
PVC	Plant vulnerability curve
SSP	Species specific parametrization
TWD	Tree water deficit

Acknowledgments

This work is supported by the Luxembourg National Research Fund (FNR) CORE program (grant no. FNR/CORE/C19/SR/13652816/CAPACITY). GF and RS acknowledges the financial support of the FNR (grant no. AFR/STEP-UP ID 12546983, grant no. FNR/CORE/C17/SR/11702136/EFFECT). The authors would like to thank Jérôme Juilleret for his invaluable field assistance in the collection of sap flow and dendrometer data and Lindsey Stokes for proofreading the manuscript.

Open Research

The COSMO-REA6 data used to complete the missing data for the atmospheric forcing in the study are available from the opendata-FTP server at DWD (https://opendata.dwd.de/climate_environment/REA/COSMO_REA6/) (COSMO-REA6, 2019).

CLM5.0 is publicly available through the Community Terrestrial System Model (CTSM) git repository (Tag name: release-clm5.0.34) via https://github.com/ESCOMP/ctsm (CTSM, 2017/2022). All analyses were done with the open source software R (R Core Team, 2022). The atmospheric forcing, daily averages of sap flow and dendrometer data, the results of the numerical experiments, and the R scripts for post-processing the data are available from ZENODO repository via https://doi.org/10.5281/zenodo.7306884 with a Creative Commons Attribution 4.0 International license for the files (Jiménez-Rodríguez, 2023).

References

ACT. (2020). LiDAR 2019—Relevé 3D du territoire luxembourgeois. Administration du Cadastre et de la Topographie (ACT). Le Gouvernement du Grand-Duché de Luxembourg. https://data.public.lu/fr/datasets/lidar-2019-modele-numerique-du-terrain/

Ali, A. A., Fan, Y., Corre, M. D., Kotowska, M. M., Preuss-Hassler, E., Cahyo, A. N., Moyano, F. E., Stiegler, C., Röll, A., Meijide, A., Olchev, A., Ringeler, A., Leuschner, C., Ariani, R., June, T., Tarigan, S., Kreft, H., Hölscher, D., Xu, C., … Knohl, A. (2022). Implementing a New Rubber Plant Functional Type in the Community Land Model (CLM5) Improves Accuracy of Carbon and Water Flux Estimation. Land, 11(2), Article 2. https://doi.org/10.3390/land11020183

Aranda, I., Gil, L., & Pardos, J. A. (2005). Seasonal changes in apparent hydraulic conductance and their implications for water use of European beech (Fagus sylvatica L.) and sessile oak [Quercus petraea (Matt.) Liebl] in South Europe. Plant Ecology, 179(2), 155–167. https://doi.org/10.1007/s11258-004-7007-1

Arend, M., Link, R. M., Patthey, R., Hoch, G., Schuldt, B., & Kahmen, A. (2021). Rapid hydraulic collapse as cause of drought-induced mortality in conifers. Proceedings of the National Academy of Sciences, 118(16), e2025251118. https://doi.org/10.1073/pnas.2025251118

Bär, A., Nardini, A., & Mayr, S. (2018). Post-fire effects in xylem hydraulics of Picea abies, Pinus sylvestris and Fagus sylvatica. New Phytologist, 217(4), 1484–1493. https://doi.org/10.1111/nph.14916

Barbati, A., Marchetti, M., Chirici, G., & Corona, P. (2014). European Forest Types and Forest Europe SFM indicators: Tools for monitoring progress on forest biodiversity conservation. Forest Ecology and Management, 321, 145–157. https://doi.org/10.1016/j.foreco.2013.07.004

Bento, V. A., Gouveia, C. M., DaCamara, C. C., Libonati, R., & Trigo, I. F. (2020). The roles of NDVI and Land Surface Temperature when using the Vegetation Health Index over dry regions. Global and Planetary Change, 190, 103198. https://doi.org/10.1016/j.gloplacha.2020.103198

Birch, L., Schwalm, C. R., Natali, S., Lombardozzi, D., Keppel-Aleks, G., Watts, J., Lin, X., Zona, D., Oechel, W., Sachs, T., Black, T. A., & Rogers, B. M. (2021). Addressing biases in Arctic–boreal carbon cycling in the Community Land Model Version 5. Geoscientific Model Development, 14(6), 3361–3382. https://doi.org/10.5194/gmd-14-3361-2021

Bohrer, G., & Missik, J. E. C. (2022). Formulation of a Consistent Multi-Species Canopy Description for Hydrodynamic Models Embedded in Large-Scale Land-Surface Representations of Mixed-Forests. Journal of Geophysical Research: Biogeosciences, 127(7), e2022JG006982. https://doi.org/10.1029/2022JG006982

Bonan, G. B., Williams, M., Fisher, R. A., & Oleson, K. W. (2014). Modeling stomatal conductance in the earth system: Linking leaf water-use efficiency and water transport along the soil–plant–atmosphere continuum. Geoscientific Model Development, 7(5), 2193–2222. https://doi.org/10.5194/gmd-7-2193-2014

Bosela, M., Tobin, B., Šebeň, V., Petráš, R., & Larocque, G. R. (2015). Different mixtures of Norway spruce, silver fir, and European beech modify competitive interactions in central European mature mixed forests. Canadian Journal of Forest Research, 45(11), 1577–1586. https://doi.org/10.1139/cjfr-2015-0219

Bravo-Oviedo, A., Pretzsch, H., Ammer, C., Andenmatten, E., Barbati, A., Barreiro, S., Brang, P., Bravo, F., Coll, L., Corona, P., Ouden, J. den, Ducey, M. J., Forrester, D. I., Giergiczny, M., Jacobsen, J. B., Lesinski, J., Löf, M., Mason, W. L., Matovic, B., … Zlatanov, T. (2014). European Mixed Forests: Definition and research perspectives. Forest Systems, 23(3), Article 3. https://doi.org/10.5424/fs/2014233-06256

Bréda, N., Cochard, H., Dreyer, E., & Granier, A. (1993). Water transfer in a mature oak stand (Quercuspetraea): Seasonal evolution and effects of a severe drought. Canadian Journal of Forest Research, 23(6), 1136–1143. https://doi.org/10.1139/x93-144

Brinkmann, N., Eugster, W., Buchmann, N., & Kahmen, A. (2019). Species-specific differences in water uptake depth of mature temperate trees vary with water availability in the soil. Plant Biology, 21(1), 71–81. https://doi.org/10.1111/plb.12907

Brinkmann, N., Eugster, W., Zweifel, R., Buchmann, N., & Kahmen, A. (2016). Temperate tree species show identical response in tree water deficit but different sensitivities in sap flow to summer soil drying. Tree Physiology, 36(12), 1508–1519. https://doi.org/10.1093/treephys/tpw062

Brodersen, C. R., Roddy, A. B., Wason, J. W., & McElrone, A. J. (2019). Functional Status of Xylem Through Time. Annual Review of Plant Biology, 70(1), 407–433. https://doi.org/10.1146/annurev-arplant-050718-100455

Buras, A., & Menzel, A. (2019). Projecting Tree Species Composition Changes of European Forests for 2061–2090 Under RCP 4.5 and RCP 8.5 Scenarios. Frontiers in Plant Science, 9. https://www.frontiersin.org/articles/10.3389/fpls.2018.01986

Chaney, N. W., Herman, J. D., Ek, M. B., & Wood, E. F. (2016). Deriving global parameter estimates for the Noah land surface model using FLUXNET and machine learning. Journal of Geophysical Research: Atmospheres, 121(22), 13,218-13,235. https://doi.org/10.1002/2016JD024821

Chatanga, P., & Sieben, E. J. J. (2020). Variation in Plant Functional Composition of the Afromontane Palustrine Wetlands Along an Altitudinal Gradient in Lesotho. Wetlands, 40(6), 2539–2552. https://doi.org/10.1007/s13157-020-01345-x

Choat, B., Jansen, S., Brodribb, T. J., Cochard, H., Delzon, S., Bhaskar, R., Bucci, S. J., Feild, T. S., Gleason, S. M., Hacke, U. G., Jacobsen, A. L., Lens, F., Maherali, H., Martínez-Vilalta,

J., Mayr, S., Mencuccini, M., Mitchell, P. J., Nardini, A., Pittermann, J., … Zanne, A. E. (2012). Global convergence in the vulnerability of forests to drought. Nature, 491(7426), 752–755. https://doi.org/10.1038/nature11688

Chu, H., Luo, X., Ouyang, Z., Chan, W. S., Dengel, S., Biraud, S. C., Torn, M. S., Metzger, S., Kumar, J., Arain, M. A., Arkebauer, T. J., Baldocchi, D., Bernacchi, C., Billesbach, D., Black, T. A., Blanken, P. D., Bohrer, G., Bracho, R., Brown, S., … Zona, D. (2021). Representativeness of Eddy-Covariance flux footprints for areas surrounding AmeriFlux sites. Agricultural and Forest Meteorology, 301–302, 108350. https://doi.org/10.1016/j.agrformet.2021.108350

Colin Prentice, I., Sykes, M. T., & Cramer, W. (1993). A simulation model for the transient effects of climate change on forest landscapes. Ecological Modelling, 65(1), 51–70. https://doi.org/10.1016/0304-3800(93)90126-D

COSMO-REA6. (2019). COSMO Regional Reanalysis (COSMO-REA6) [Dataset]. https://reanalysis.meteo.uni-bonn.de/?COSMO-REA6

Cranko Page, J., Abramowitz, G., De Kauwe, Martin. G., & Pitman, A. J. (2024). Are Plant Functional Types Fit for Purpose? Geophysical Research Letters, 51(1), e2023GL104962. https://doi.org/10.1029/2023GL104962

CTSM. (2022). Community Terrestrial Systems Model (includes the Community Land Model of CESM) [CTSM] [Software] [Fortran]. Earth System Community Modeling Portal. https://github.com/ESCOMP/CTSM (Original work published 2017)

de Rigo, D., Caudullo, G., Houston Durrant, T., & San-Miguel-Ayanz, J. (2016). The European Atlas of Forest Tree Species: Modelling, data and information on forest tree species. In: San-Miguel-Ayanz, J., de Rigo, D., Caudullo, G., Houston Durrant, T., Mauri, A. (Eds.), European Atlas of Forest Tree Species. Publ. Off. EU, Luxembourg, pp. E01aa69+.

del Río, M., Pretzsch, H., Alberdi, I., Bielak, K., Bravo, F., Brunner, A., Condés, S., Ducey, M. J., Fonseca, T., von Lüpke, N., Pach, M., Peric, S., Perot, T., Souidi, Z., Spathelf, P., Sterba, H., Tijardovic, M., Tomé, M., Vallet, P., & Bravo-Oviedo, A. (2018). Characterization of Mixed Forests. In A. Bravo-Oviedo, H. Pretzsch, & M. del Río (Eds.), Dynamics, Silviculture and Management of Mixed Forests (pp. 27–71). Springer International Publishing. https://doi.org/10.1007/978-3-319-91953-9_2

Dietrich, L., Delzon, S., Hoch, G., & Kahmen, A. (2019). No role for xylem embolism or carbohydrate shortage in temperate trees during the severe 2015 drought. Journal of Ecology, 107(1), 334–349. https://doi.org/10.1111/1365-2745.13051

Dietrich, L., Zweifel, R., & Kahmen, A. (2018). Daily stem diameter variations can predict the canopy water status of mature temperate trees. Tree Physiology, 38(7), 941–952. https://doi.org/10.1093/treephys/tpy023

Dixon, M. A., & Tyree, M. T. (1984). A new stem hygrometer, corrected for temperature gradients and calibrated against the pressure bomb. Plant, Cell & Environment, 7(9), 693–697. https://doi.org/10.1111/1365-3040.ep11572454

Domec, J.-C., Lachenbruch, B., Pruyn, M. L., & Spicer, R. (2012). Effects of age-related increases in sapwood area, leaf area, and xylem conductivity on height-related hydraulic

costs in two contrasting coniferous species. Annals of Forest Science, 69(1), 17–27. https://doi.org/10.1007/s13595-011-0154-3

Drew, D. M., Richards, A. E., Downes, G. M., Cook, G. D., & Baker, P. (2011). The development of seasonal tree water deficit in Callitris intratropica. Tree Physiology, 31(9), 953–964. https://doi.org/10.1093/treephys/tpr031

Druel, A., Peylin, P., Krinner, G., Ciais, P., Viovy, N., Peregon, A., Bastrikov, V., Kosykh, N., & Mironycheva-Tokareva, N. (2017). Towards a more detailed representation of high-latitude vegetation in the global land surface model ORCHIDEE (ORC-HL-VEGv1.0). Geoscientific Model Development, 10(12), 4693–4722. https://doi.org/10.5194/gmd-10-4693-2017

Duveiller, G., Fasbender, D., & Meroni, M. (2016). Revisiting the concept of a symmetric index of agreement for continuous datasets. Scientific Reports, 6(1), Article 1. https://doi.org/10.1038/srep19401

EDO. (2023). Trend Viewer—European Drought Observatory—JRC European Commission. https://edo.jrc.ec.europa.eu/edov2/php/index.php?id=1059

Eller, C. B., Rowland, L., Mencuccini, M., Rosas, T., Williams, K., Harper, A., Medlyn, B. E., Wagner, Y., Klein, T., Teodoro, G. S., Oliveira, R. S., Matos, I. S., Rosado, B. H. P., Fuchs, K., Wohlfahrt, G., Montagnani, L., Meir, P., Sitch, S., & Cox, P. M. (2020). Stomatal optimization based on xylem hydraulics (SOX) improves land surface model simulation of vegetation responses to climate. New Phytologist, 226(6), 1622–1637. https://doi.org/10.1111/nph.16419

Fabiani, G., Schoppach, R., Penna, D., & Klaus, J. (2022). Transpiration patterns and water use strategies of beech and oak trees along a hillslope. Ecohydrology, 15(2), e2382. https://doi.org/10.1002/eco.2382

Felton, A., Lindbladh, M., Brunet, J., & Fritz, Ö. (2010). Replacing coniferous monocultures with mixed-species production stands: An assessment of the potential benefits for forest biodiversity in northern Europe. Forest Ecology and Management, 260(6), 939–947. https://doi.org/10.1016/j.foreco.2010.06.011

Fernández-de-Uña, L., Cañellas, I., & Gea-Izquierdo, G. (2015). Stand Competition Determines How Different Tree Species Will Cope with a Warming Climate. PLOS ONE, 10(3), e0122255. https://doi.org/10.1371/journal.pone.0122255

Ford, K. R., Breckheimer, I. K., Franklin, J. F., Freund, J. A., Kroiss, S. J., Larson, A. J., Theobald, E. J., & HilleRisLambers, J. (2017). Competition alters tree growth responses to climate at individual and stand scales. Canadian Journal of Forest Research, 47(1), 53–62. https://doi.org/10.1139/cjfr-2016-0188

FOREST EUROPE. (2020). State of Europe's Forests 2020. Ministerial Conference on the Protection of Forests in Europe - FOREST EUROPE. Liaison Unit Bratislava. https://foresteurope.org/state-of-europes-forests/

Forrester, D. I., Limousin, J.-M., & Pfautsch, S. (2022). The relationship between tree size and tree water-use: Is competition for water size-symmetric or size-asymmetric? Tree Physiology, 42(10), 1916–1927. https://doi.org/10.1093/treephys/tpac018

Fry, E. L., De Long, J. R., Álvarez Garrido, L., Alvarez, N., Carrillo, Y., Castañeda-Gómez, L., Chomel, M., Dondini, M., Drake, J. E., Hasegawa, S., Hortal, S., Jackson, B. G., Jiang, M., Lavallee, J. M., Medlyn, B. E., Rhymes, J., Singh, B. K., Smith, P., Anderson, I. C., … Johnson, D. (2019). Using plant, microbe, and soil fauna traits to improve the predictive power of biogeochemical models. Methods in Ecology and Evolution, 10(1), 146–157. https://doi.org/10.1111/2041-210X.13092

Fukuzawa, K., Shibata, H., Takagi, K., Satoh, F., Koike, T., & Sasa, K. (2007). Vertical distribution and seasonal pattern of fine-root dynamics in a cool–temperate forest in northern Japan: Implication of the understory vegetation, Sasa dwarf bamboo. Ecological Research, 22(3), 485–495. https://doi.org/10.1007/s11284-006-0031-y

Glaser, B., Klaus, J., Frei, S., Frentress, J., Pfister, L., & Hopp, L. (2016). On the value of surface saturated area dynamics mapped with thermal infrared imagery for modeling the hillslope-riparian-stream continuum. Water Resources Research, 52(10), 8317–8342. https://doi.org/10.1002/2015WR018414

Gong, H., Yao, F., & Gao, J. (2020). Succession of a broad-leaved Korean pine mixed forest: Functional plant trait composition. Global Ecology and Conservation, 22, e00950. https://doi.org/10.1016/j.gecco.2020.e00950

Guan, X., Werner, J., Cao, K.-F., Pereira, L., Kaack, L., McAdam, S. a. M., & Jansen, S. (2022). Stem and leaf xylem of angiosperm trees experiences minimal embolism in temperate forests during two consecutive summers with moderate drought. Plant Biology, 24(7), 1208–1223. https://doi.org/10.1111/plb.13384

Hacke, U., & Sauter, J. J. (1995). Vulnerability of xylem to embolism in relation to leaf water potential and stomatal conductance in Fagus sylvatica f. Purpurea and Populus balsamifera. Journal of Experimental Botany, 46(9), 1177–1183. https://doi.org/10.1093/jxb/46.9.1177

Haeni, M., Knüsel, S., Peters, R. L., & Zweifel, R. (2020). Treenetproc—Clean, process and visualise dendrometer data. R package version 0.1.4. Github repository: Https://github.com/treenet/treenetproc. Treenetproc - Clean, Process and Visualise Dendrometer Data. R Package Version 0.1.4. Github Repository: Https://Github.Com/Treenet/Treenetproc. https://github.com/treenet/treenetproc

Hajek, P., Link, R. M., Nock, C. A., Bauhus, J., Gebauer, T., Gessler, A., Kovach, K., Messier, C., Paquette, A., Saurer, M., Scherer-Lorenzen, M., Rose, L., & Schuldt, B. (2022). Mutually inclusive mechanisms of drought-induced tree mortality. Global Change Biology, 28(10), 3365–3378. https://doi.org/10.1111/gcb.16146

Hammond, W. M., Williams, A. P., Abatzoglou, J. T., Adams, H. D., Klein, T., López, R., Sáenz-Romero, C., Hartmann, H., Breshears, D. D., & Allen, C. D. (2022). Global field observations of tree die-off reveal hotter-drought fingerprint for Earth's forests. Nature Communications, 13(1), Article 1. https://doi.org/10.1038/s41467-022-29289-2

Han, X., Huang, J., & Zang, R. (2022). Soil nutrients and climate seasonality drive differentiation of ecological strategies of species in forests across four climatic zones. Plant and Soil, 473(1), 517–531. https://doi.org/10.1007/s11104-022-05303-w

Harper, A. B., Williams, K. E., McGuire, P. C., Duran Rojas, M. C., Hemming, D., Verhoef, A., Huntingford, C., Rowland, L., Marthews, T., Breder Eller, C., Mathison, C., Nobrega, R.

L. B., Gedney, N., Vidale, P. L., Otu-Larbi, F., Pandey, D., Garrigues, S., Wright, A., Slevin, D., … Wohlfahrt, G. (2021). Improvement of modeling plant responses to low soil moisture in JULESvn4.9 and evaluation against flux tower measurements. Geoscientific Model Development, 14(6), 3269–3294. https://doi.org/10.5194/gmd-14-3269-2021

Hartley, A. J., MacBean, N., Georgievski, G., & Bontemps, S. (2017). Uncertainty in plant functional type distributions and its impact on land surface models. Remote Sensing of Environment, 203, 71–89. https://doi.org/10.1016/j.rse.2017.07.037

Hartzell, S., Bartlett, M. S., & Porporato, A. (2017). The role of plant water storage and hydraulic strategies in relation to soil moisture availability. Plant and Soil, 419(1), 503–521. https://doi.org/10.1007/s11104-017-3341-7

He, X., Pan, M., Wei, Z., Wood, E. F., & Sheffield, J. (2020). A Global Drought and Flood Catalogue from 1950 to 2016. Bulletin of the American Meteorological Society, 101(5), E508–E535. https://doi.org/10.1175/BAMS-D-18-0269.1

Hissler, C., Martínez-Carreras, N., Barnich, F., Gourdol, L., Iffly, J. F., Juilleret, J., Klaus, J., & Pfister, L. (2021). The Weierbach experimental catchment in Luxembourg: A decade of critical zone monitoring in a temperate forest - from hydrological investigations to ecohydrological perspectives. Hydrological Processes, 35(5), e14140. https://doi.org/10.1002/hyp.14140

Hochberg, U., Rockwell, F. E., Holbrook, N. M., & Cochard, H. (2018). Iso/Anisohydry: A Plant–Environment Interaction Rather Than a Simple Hydraulic Trait. Trends in Plant Science, 23(2), 112–120. https://doi.org/10.1016/j.tplants.2017.11.002

Hufkens, K. (2022). MODISTools. https://cran.r-project.org/web/packages/MODISTools/vignettes/modistools-vignette.html

Jactel, H., Bauhus, J., Boberg, J., Bonal, D., Castagneyrol, B., Gardiner, B., Gonzalez-Olabarria, J. R., Koricheva, J., Meurisse, N., & Brockerhoff, E. G. (2017). Tree Diversity Drives Forest Stand Resistance to Natural Disturbances. Current Forestry Reports, 3(3), 223–243. https://doi.org/10.1007/s40725-017-0064-1

Jiménez-Rodríguez, C. D. (2023). Data Repository: Land surface modelling activities at Weierbach catchment. [Dataset] [dataset]. https://doi.org/10.5281/zenodo.7306884

Jiménez-Rodríguez, C. D., Sulis, M., & Schymanski, S. (2022). Exploring the role of bedrock representation on plant transpiration response during dry periods at four forested sites in Europe. Biogeosciences, 19(14), 3395–3423. https://doi.org/10.5194/bg-19-3395-2022

Jiménez-Rodríguez, C. D., Sulis, M., & Schymanski, S. (2024). The role of the intraspecific variability of hydraulic traits for modelling the plant water use in different European forest ecosystems. Accepted on 25 January 2024. In Press. Journal of Advances in Modeling Earth Systems. https://doi.org/10.1029/2022MS003494

Kannenberg, S. A., Novick, K. A., Alexander, M. R., Maxwell, J. T., Moore, D. J. P., Phillips, R. P., & Anderegg, W. R. L. (2019). Linking drought legacy effects across scales: From leaves to tree rings to ecosystems. Global Change Biology, 25(9), 2978–2992. https://doi.org/10.1111/gcb.14710

Kannenberg, S. A., Novick, K. A., & Phillips, R. P. (2019). Anisohydric behavior linked to persistent hydraulic damage and delayed drought recovery across seven North American tree species. New Phytologist, 222(4), 1862–1872. https://doi.org/10.1111/nph.15699

Kannenberg, S. A., Schwalm, C. R., & Anderegg, W. R. L. (2020). Ghosts of the past: How drought legacy effects shape forest functioning and carbon cycling. Ecology Letters, 23(5), 891–901. https://doi.org/10.1111/ele.13485

Ke, Y., Leung, L. R., Huang, M., & Li, H. (2013). Enhancing the representation of subgrid land surface characteristics in land surface models. Geoscientific Model Development, 6(5), 1609–1622. https://doi.org/10.5194/gmd-6-1609-2013

Kennedy, D., Swenson, S., Oleson, K. W., Lawrence, D. M., Fisher, R., Lola da Costa, A. C., & Gentine, P. (2019). Implementing Plant Hydraulics in the Community Land Model, Version 5. Journal of Advances in Modeling Earth Systems, 11(2), 485–513. https://doi.org/10.1029/2018MS001500

Klein, T., Zeppel, M. J. B., Anderegg, W. R. L., Bloemen, J., De Kauwe, M. G., Hudson, P., Ruehr, N. K., Powell, T. L., von Arx, G., & Nardini, A. (2018). Xylem embolism refilling and resilience against drought-induced mortality in woody plants: Processes and trade-offs. Ecological Research, 33(5), 839–855. https://doi.org/10.1007/s11284-018-1588-y

Knüsel, S., Peters, R. L., Haeni, M., Wilhelm, M., & Zweifel, R. (2021). Processing and Extraction of Seasonal Tree Physiological Parameters from Stem Radius Time Series. Forests, 12(6), Article 6. https://doi.org/10.3390/f12060765

Laughlin, D. C., Siefert, A., Fleri, J. R., Tumber-Dávila, S. J., Hammond, W. M., Sabatini, F. M., Damasceno, G., Aubin, I., Field, R., Hatim, M. Z., Jansen, S., Lenoir, J., Lens, F., McCarthy, J. K., Niinemets, Ü., Phillips, O. L., Attorre, F., Bergeron, Y., Bruun, H. H., … Bruelheide, H. (2023). Rooting depth and xylem vulnerability are independent woody plant traits jointly selected by aridity, seasonality, and water table depth. New Phytologist, n/a(n/a). https://doi.org/10.1111/nph.19276

Lavaysse, C., Cammalleri, C., Dosio, A., van der Schrier, G., Toreti, A., & Vogt, J. (2018). Towards a monitoring system of temperature extremes in Europe. Natural Hazards and Earth System Sciences, 18(1), 91–104. https://doi.org/10.5194/nhess-18-91-2018

Lavoir, A.-V., Staudt, M., Schnitzler, J. P., Landais, D., Massol, F., Rocheteau, A., Rodriguez, R., Zimmer, I., & Rambal, S. (2009). Drought reduced monoterpene emissions from the evergreen Mediterranean oak Quercus ilex: Results from a throughfall displacement experiment. Biogeosciences, 6(7), 1167–1180. https://doi.org/10.5194/bg-6-1167-2009

Lawrence, D. M., Fisher, R. A., Koven, C. D., Oleson, K. W., Swenson, S. C., Bonan, G., Collier, N., Ghimire, B., van Kampenhout, L., Kennedy, D., Kluzek, E., Lawrence, P. J., Li, F., Li, H., Lombardozzi, D., Riley, W. J., Sacks, W. J., Shi, M., Vertenstein, M., … Zeng, X. (2019). The Community Land Model Version 5: Description of New Features, Benchmarking, and Impact of Forcing Uncertainty. Journal of Advances in Modeling Earth Systems, 11(12), 4245–4287. https://doi.org/10.1029/2018MS001583

Lemoine, D., Cochard, H., & Granier, A. (2002). Within crown variation in hydraulic architecture in beech (Fagus sylvatica L): Evidence for a stomatal control of xylem embolism. Annals of Forest Science, 59(1), 19–27. https://doi.org/10.1051/forest:2001002

Li, J., Bevacqua, E., Wang, Z., Sitch, S., Arora, V., Arneth, A., Jain, A. K., Goll, D., Tian, H., & Zscheischler, J. (2023). Hydroclimatic extremes contribute to asymmetric trends in ecosystem productivity loss. Communications Earth & Environment, 4(1), 197. https://doi.org/10.1038/s43247-023-00869-4

Li, L., Yang, Z.-L., Matheny, A. M., Zheng, H., Swenson, S. C., Lawrence, D. M., Barlage, M., Yan, B., McDowell, N. G., & Leung, L. R. (2021a). Representation of Plant Hydraulics in the Noah-MP Land Surface Model: Model Development and Multiscale Evaluation. Journal of Advances in Modeling Earth Systems, 13(4), e2020MS002214. https://doi.org/10.1029/2020MS002214

Li, L., Yang, Z.-L., Matheny, A. M., Zheng, H., Swenson, S. C., Lawrence, D. M., Barlage, M., Yan, B., McDowell, N. G., & Leung, L. R. (2021b). Representation of Plant Hydraulics in the Noah-MP Land Surface Model: Model Development and Multiscale Evaluation. Journal of Advances in Modeling Earth Systems, 13(4), e2020MS002214. https://doi.org/10.1029/2020MS002214

Lin, Y.-S., Medlyn, B. E., Duursma, R. A., Prentice, I. C., Wang, H., Baig, S., Eamus, D., de Dios, V. R., Mitchell, P., Ellsworth, D. S., de Beeck, M. O., Wallin, G., Uddling, J., Tarvainen, L., Linderson, M.-L., Cernusak, L. A., Nippert, J. B., Ocheltree, T. W., Tissue, D. T., … Wingate, L. (2015). Optimal stomatal behaviour around the world. Nature Climate Change, 5(5), Article 5. https://doi.org/10.1038/nclimate2550

Lobo, A., Torres-Ruiz, J. M., Burlett, R., Lemaire, C., Parise, C., Francioni, C., Truffaut, L., Tomášková, I., Hansen, J. K., Kjær, E. D., Kremer, A., & Delzon, S. (2018). Assessing inter- and intraspecific variability of xylem vulnerability to embolism in oaks. Forest Ecology and Management, 424, 53–61. https://doi.org/10.1016/j.foreco.2018.04.031

López, B., Sabaté, S., & Gracia, C. A. (2001). Annual and seasonal changes in fine root biomass of a Quercus ilex L. forest. Plant and Soil, 230(1), 125–134. https://doi.org/10.1023/A:1004824719377

Lutz, J. A., Larson, A. J., Freund, J. A., Swanson, M. E., & Bible, K. J. (2013). The Importance of Large-Diameter Trees to Forest Structural Heterogeneity. PLOS ONE, 8(12), e82784. https://doi.org/10.1371/journal.pone.0082784

Ma, Q., Su, Y., Niu, C., Ma, Q., Hu, T., Luo, X., Tai, X., Qiu, T., Zhang, Y., Bales, R. C., Liu, L., Kelly, M., & Guo, Q. (2023). Tree mortality during long-term droughts is lower in structurally complex forest stands. Nature Communications, 14(1), Article 1. https://doi.org/10.1038/s41467-023-43083-8

Martínez-Carreras, N., Hissler, C., Gourdol, L., Klaus, J., Juilleret, J., Iffly, J. F., & Pfister, L. (2016). Storage controls on the generation of double peak hydrographs in a forested headwater catchment. Journal of Hydrology, 543, 255–269. https://doi.org/10.1016/j.jhydrol.2016.10.004

McDowell, N. G., Allen, C. D., Anderson-Teixeira, K., Aukema, B. H., Bond-Lamberty, B., Chini, L., Clark, J. S., Dietze, M., Grossiord, C., Hanbury-Brown, A., Hurtt, G. C., Jackson, R. B., Johnson, D. J., Kueppers, L., Lichstein, J. W., Ogle, K., Poulter, B., Pugh, T. A. M., Seidl, R., … Xu, C. (2020). Pervasive shifts in forest dynamics in a changing world. Science, 368(6494), eaaz9463. https://doi.org/10.1126/science.aaz9463

Meinzer, F. C., & McCulloh, K. A. (2013). Xylem recovery from drought-induced embolism: Where is the hydraulic point of no return? Tree Physiology, 33(4), 331–334. https://doi.org/10.1093/treephys/tpt022

Mina, M., Huber, M. O., Forrester, D. I., Thürig, E., & Rohner, B. (2018). Multiple factors modulate tree growth complementarity in Central European mixed forests. Journal of Ecology, 106(3), 1106–1119. https://doi.org/10.1111/1365-2745.12846

Mohanty, B. P., Cosh, M. H., Lakshmi, V., & Montzka, C. (2017). Soil Moisture Remote Sensing: State-of-the-Science. Vadose Zone Journal, 16(1), 1–9. https://doi.org/10.2136/vzj2016.10.0105

Muñoz Sabater, J. (2019). ERA5-Land hourly data from 1981 to present. Copernicus Climate Change Service (C3S) Climate Data Store (CDS). https://doi.org/10.24381/cds.e2161bac

Muñoz Sabater, J. (2021). ERA5-Land hourly data from 1950 to 1980. Copernicus Climate Change Service (C3S) Climate Data Store (CDS). https://doi.org/10.24381/cds.e2161bac

Nascimbene, J., Thor, G., & Nimis, P. L. (2013). Effects of forest management on epiphytic lichens in temperate deciduous forests of Europe – A review. Forest Ecology and Management, 298, 27–38. https://doi.org/10.1016/j.foreco.2013.03.008

NOAA-ESRL. (2022). Weclome to the Mauna Loa Observatory. (Webpage). Retrieved from https://www.esrl.noaa.gov/gmd/obop/mlo/ [Daily CO2].

Obladen, N., Dechering, P., Skiadaresis, G., Tegel, W., Keßler, J., Höllerl, S., Kaps, S., Hertel, M., Dulamsuren, C., Seifert, T., Hirsch, M., & Seim, A. (2021). Tree mortality of European beech and Norway spruce induced by 2018-2019 hot droughts in central Germany. Agricultural and Forest Meteorology, 307, 108482. https://doi.org/10.1016/j.agrformet.2021.108482

ORNL DAAC. (2018). MODIS and VIIRS Land Product Subsets RESTful Web Service. ORNL DAAC, Oak Ridge, Tennessee, USA. https://doi.org/10.3334/ORNLDAAC/1600

pch.vector. (2023). Tree crowns image set by pch.vector on Freepik. https://www.freepik.com/free-vector/tree-crowns-set_13683715.htm#query=tree%20crown&position=0&from_view=search&track=ais

Peiffer, M., Bréda, N., Badeau, V., & Granier, A. (2014). Disturbances in European beech water relation during an extreme drought. Annals of Forest Science, 71(7), Article 7. https://doi.org/10.1007/s13595-014-0383-3

Pelletier, J. D., Broxton, P. D., Hazenberg, P., Zeng, X., Troch, P. A., Niu, G.-Y., Williams, Z., Brunke, M. A., & Gochis, D. (2016). A gridded global data set of soil, intact regolith, and sedimentary deposit thicknesses for regional and global land surface modeling. Journal of Advances in Modeling Earth Systems, 8(1), 41–65. https://doi.org/10.1002/2015MS000526

Perona, P., Flury, R., Barry, D. A., & Schwarz, M. (2022). Tree root distribution modelling in different environmental conditions. Ecological Engineering, 185, 106811. https://doi.org/10.1016/j.ecoleng.2022.106811

Pfister, L., Martínez-Carreras, N., Hissler, C., Klaus, J., Carrer, G. E., Stewart, M. K., & McDonnell, J. J. (2017). Bedrock geology controls on catchment storage, mixing, and

release: A comparative analysis of 16 nested catchments. Hydrological Processes, 31(10), 1828–1845. https://doi.org/10.1002/hyp.11134

Poulter, B., MacBean, N., Hartley, A., Khlystova, I., Arino, O., Betts, R., Bontemps, S., Boettcher, M., Brockmann, C., Defourny, P., Hagemann, S., Herold, M., Kirches, G., Lamarche, C., Lederer, D., Ottlé, C., Peters, M., & Peylin, P. (2015). Plant functional type classification for earth system models: Results from the European Space Agency's Land Cover Climate Change Initiative. Geoscientific Model Development, 8(7), 2315–2328. https://doi.org/10.5194/gmd-8-2315-2015

Poyatos, R., Granda, V., Flo, V., Adams, M. A., Adorján, B., Aguadé, D., Aidar, M. P. M., Allen, S., Alvarado-Barrientos, M. S., Anderson-Teixeira, K. J., Aparecido, L. M., Arain, M. A., Aranda, I., Asbjornsen, H., Baxter, R., Beamesderfer, E., Berry, Z. C., Berveiller, D., Blakely, B., … Martínez-Vilalta, J. (2021). Global transpiration data from sap flow measurements: The SAPFLUXNET database. Earth System Science Data, 13(6), 2607–2649. https://doi.org/10.5194/essd-13-2607-2021

Prăvălie, R., Sîrodoev, I., Nita, I.-A., Patriche, C., Dumitraşcu, M., Roşca, B., Tişcovschi, A., Bandoc, G., Săvulescu, I., Mănoiu, V., & Birsan, M.-V. (2022). NDVI-based ecological dynamics of forest vegetation and its relationship to climate change in Romania during 1987–2018. Ecological Indicators, 136, 108629. https://doi.org/10.1016/j.ecolind.2022.108629

Preisler, Y., Hölttä, T., Grünzweig, J. M., Oz, I., Tatarinov, F., Ruehr, N. K., Rotenberg, E., & Yakir, D. (2022). The importance of tree internal water storage under drought conditions. Tree Physiology, 42(4), 771–783. https://doi.org/10.1093/treephys/tpab144

Pretzsch, H. (2019). The Effect of Tree Crown Allometry on Community Dynamics in Mixed-Species Stands versus Monocultures. A Review and Perspectives for Modeling and Silvicultural Regulation. Forests, 10(9), Article 9. https://doi.org/10.3390/f10090810

Pretzsch, H., Schütze, G., & Uhl, E. (2013). Resistance of European tree species to drought stress in mixed versus pure forests: Evidence of stress release by inter-specific facilitation. Plant Biology, 15(3), 483–495. https://doi.org/10.1111/j.1438-8677.2012.00670.x

R Core Team. (2022). R: A Language and Environment for Statistical Computing, R Foundation for Statistical Computing, Vienna, Austria. [Software]. https://www.R-project.org

Raczka, B., Hoar, T. J., Duarte, H. F., Fox, A. M., Anderson, J. L., Bowling, D. R., & Lin, J. C. (2021). Improving CLM5.0 Biomass and Carbon Exchange Across the Western United States Using a Data Assimilation System. Journal of Advances in Modeling Earth Systems, 13(7), e2020MS002421. https://doi.org/10.1029/2020MS002421

Rosner, S., Johnson, D. M., Voggeneder, K., & Domec, J.-C. (2019). The conifer-curve: Fast prediction of hydraulic conductivity loss and vulnerability to cavitation. Annals of Forest Science, 76(3), Article 3. https://doi.org/10.1007/s13595-019-0868-1

Sabot, M. E. B., De Kauwe, M. G., Pitman, A. J., Medlyn, B. E., Verhoef, A., Ukkola, A. M., & Abramowitz, G. (2020). Plant profit maximization improves predictions of European forest responses to drought. New Phytologist, 226(6), 1638–1655. https://doi.org/10.1111/nph.16376

Schäfer, C., Rötzer, T., Thurm, E. A., Biber, P., Kallenbach, C., & Pretzsch, H. (2019). Growth and Tree Water Deficit of Mixed Norway Spruce and European Beech at Different Heights in a Tree and under Heavy Drought. Forests, 10(7), Article 7. https://doi.org/10.3390/f10070577

Schoppach, R., Chun, K. P., He, Q., Fabiani, G., & Klaus, J. (2021). Species-specific control of DBH and landscape characteristics on tree-to-tree variability of sap velocity. Agricultural and Forest Meteorology, 307, 108533. https://doi.org/10.1016/j.agrformet.2021.108533

Schuldt, B., Buras, A., Arend, M., Vitasse, Y., Beierkuhnlein, C., Damm, A., Gharun, M., Grams, T. E. E., Hauck, M., Hajek, P., Hartmann, H., Hiltbrunner, E., Hoch, G., Holloway-Phillips, M., Körner, C., Larysch, E., Lübbe, T., Nelson, D. B., Rammig, A., … Kahmen, A. (2020). A first assessment of the impact of the extreme 2018 summer drought on Central European forests. Basic and Applied Ecology, 45, 86–103. https://doi.org/10.1016/j.baae.2020.04.003

Senf, C., Buras, A., Zang, C. S., Rammig, A., & Seidl, R. (2020). Excess forest mortality is consistently linked to drought across Europe. Nature Communications, 11(1), 6200. https://doi.org/10.1038/s41467-020-19924-1

Shekhar, A., Hörtnagl, L., Paul-Limoges, E., Etzold, S., Zweifel, R., Buchmann, N., & Gharun, M. (2024). Contrasting impact of extreme soil and atmospheric dryness on the functioning of trees and forests. Science of The Total Environment, 169931. https://doi.org/10.1016/j.scitotenv.2024.169931

Shrestha, P., Kurtz, W., Vogel, G., Schulz, J.-P., Sulis, M., Hendricks Franssen, H.-J., Kollet, S., & Simmer, C. (2018). Connection Between Root Zone Soil Moisture and Surface Energy Flux Partitioning Using Modeling, Observations, and Data Assimilation for a Temperate Grassland Site in Germany. Journal of Geophysical Research: Biogeosciences, 123(9), 2839–2862. https://doi.org/10.1029/2016JG003753

Sloan, B. P., Thompson, S. E., & Feng, X. (2021). Plant hydraulic transport controls transpiration sensitivity to soil water stress. Hydrology and Earth System Sciences, 25(8), 4259–4274. https://doi.org/10.5194/hess-25-4259-2021

Song, J., Miller, G. R., Cahill, A. T., Aparecido, L. M. T., & Moore, G. W. (2020). Modeling land surface processes over a mountainous rainforest in Costa Rica using CLM4.5 and CLM5. Geoscientific Model Development, 13(11), 5147–5173. https://doi.org/10.5194/gmd-13-5147-2020

Steppe, K. (2018). The potential of the tree water potential. Tree Physiology, 38(7), 937–940. https://doi.org/10.1093/treephys/tpy064

Stojnić, S., Suchocka, M., Benito-Garzón, M., Torres-Ruiz, J. M., Cochard, H., Bolte, A., Cocozza, C., Cvjetković, B., de Luis, M., Martinez-Vilalta, J., Ræbild, A., Tognetti, R., & Delzon, S. (2018). Variation in xylem vulnerability to embolism in European beech from geographically marginal populations. Tree Physiology, 38(2), 173–185. https://doi.org/10.1093/treephys/tpx128

Tesfa, T. K., & Leung, L.-Y. R. (2017). Exploring new topography-based subgrid spatial structures for improving land surface modeling. Geoscientific Model Development, 10(2), 873–888. https://doi.org/10.5194/gmd-10-873-2017

Thomas, F. M., Rzepecki, A., & Werner, W. (2022). Non-native Douglas fir (Pseudotsuga menziesii) in Central Europe: Ecology, performance and nature conservation. Forest Ecology and Management, 506, 119956. https://doi.org/10.1016/j.foreco.2021.119956

Tomasella, M., Nardini, A., Hesse, B. D., Machlet, A., Matyssek, R., & Häberle, K.-H. (2019). Close to the edge: Effects of repeated severe drought on stem hydraulics and non-structural carbohydrates in European beech saplings. Tree Physiology, 39(5), 717–728. https://doi.org/10.1093/treephys/tpy142

Torres-Rojas, L., Vergopolan, N., Herman, J. D., & Chaney, N. W. (2022). Towards an Optimal Representation of Sub-Grid Heterogeneity in Land Surface Models. Water Resources Research, 58(12), e2022WR032233. https://doi.org/10.1029/2022WR032233

Treenetproc. (2023). [R]. TreeNet. https://github.com/treenet/treenetproc (Original work published 2019)

Tuck, S. L., Phillips, H. R. P., Hintzen, R. E., Scharlemann, J. P. W., Purvis, A., & Hudson, L. N. (2014). MODISTools – downloading and processing MODIS remotely sensed data in R. Ecology and Evolution, 4(24), 4658–4668. https://doi.org/10.1002/ece3.1273

Tyree, M. T., & Ewers, F. W. (1991). The hydraulic architecture of trees and other woody plants. New Phytologist, 119(3), 345–360. https://doi.org/10.1111/j.1469-8137.1991.tb00035.x

Van Passel, J., de Keersmaecker, W., Bernardino, P. N., Jing, X., Umlauf, N., Van Meerbeek, K., & Somers, B. (2022). Climatic legacy effects on the drought response of the Amazon rainforest. Global Change Biology, 28(19), 5808–5819. https://doi.org/10.1111/gcb.16336

Venturas, M. D., Sperry, J. S., & Hacke, U. G. (2017). Plant xylem hydraulics: What we understand, current research, and future challenges. Journal of Integrative Plant Biology, 59(6), 356–389. https://doi.org/10.1111/jipb.12534

Verheijen, L. M., Aerts, R., Brovkin, V., Cavender-Bares, J., Cornelissen, J. H. C., Kattge, J., & van Bodegom, P. M. (2015). Inclusion of ecologically based trait variation in plant functional types reduces the projected land carbon sink in an earth system model. Global Change Biology, 21(8), 3074–3086. https://doi.org/10.1111/gcb.12871

Vidale, P. L., Egea, G., McGuire, P. C., Todt, M., Peters, W., Müller, O., Balan-Sarojini, B., & Verhoef, A. (2021). On the Treatment of Soil Water Stress in GCM Simulations of Vegetation Physiology. Frontiers in Environmental Science, 9. https://www.frontiersin.org/articles/10.3389/fenvs.2021.689301

Violle, C., Reich, P. B., Pacala, S. W., Enquist, B. J., & Kattge, J. (2014). The emergence and promise of functional biogeography. Proceedings of the National Academy of Sciences, 111(38), 13690–13696. https://doi.org/10.1073/pnas.1415442111

Vitasse, Y., Bottero, A., Cailleret, M., Bigler, C., Fonti, P., Gessler, A., Lévesque, M., Rohner, B., Weber, P., Rigling, A., & Wohlgemuth, T. (2019). Contrasting resistance and resilience to extreme drought and late spring frost in five major European tree species. Global Change Biology, 25(11), 3781–3792. https://doi.org/10.1111/gcb.14803

Walthert, L., Ganthaler, A., Mayr, S., Saurer, M., Waldner, P., Walser, M., Zweifel, R., & von Arx, G. (2021). From the comfort zone to crown dieback: Sequence of physiological stress

thresholds in mature European beech trees across progressive drought. Science of The Total Environment, 753, 141792. https://doi.org/10.1016/j.scitotenv.2020.141792

Wang, P., Niu, G.-Y., Fang, Y.-H., Wu, R.-J., Yu, J.-J., Yuan, G.-F., Pozdniakov, S. P., & Scott, R. L. (2018). Implementing Dynamic Root Optimization in Noah-MP for Simulating Phreatophytic Root Water Uptake. Water Resources Research, 54(3), 1560–1575. https://doi.org/10.1002/2017WR021061

Wickham, H., Romain, F., Lionel, H., & Müller, K. (2019). Dplyr: A Grammar of Data Manipulation. R package version #> 0.8.3. Https://CRAN.R-project.org/package=dplyr. https://CRAN.R-project.org/package=dplyr

Wieder, W. R., Lawrence, D. M., Fisher, R. A., Bonan, G. B., Cheng, S. J., Goodale, C. L., Grandy, A. S., Koven, C. D., Lombardozzi, D. L., Oleson, K. W., & Thomas, R. Q. (2019). Beyond Static Benchmarking: Using Experimental Manipulations to Evaluate Land Model Assumptions. Global Biogeochemical Cycles, 33(10), 1289–1309. https://doi.org/10.1029/2018GB006141

Wu, H., Fu, C., Wu, H., & Zhang, L. (2020). Plant Hydraulic Stress Strategy Improves Model Predictions of the Response of Gross Primary Productivity to Drought Across China. Journal of Geophysical Research: Atmospheres, 125(24), e2020JD033476. https://doi.org/10.1029/2020JD033476

Yu, X., Orth, R., Reichstein, M., Bahn, M., Klosterhalfen, A., Knohl, A., Koebsch, F., Migliavacca, M., Mund, M., Nelson, J. A., Stocker, B. D., Walther, S., & Bastos, A. (2022). Contrasting drought legacy effects on gross primary productivity in a mixed versus pure beech forest. Biogeosciences, 19(17), 4315–4329. https://doi.org/10.5194/bg-19-4315-2022

Zeller, L., & Pretzsch, H. (2019). Effect of forest structure on stand productivity in Central European forests depends on developmental stage and tree species diversity. Forest Ecology and Management, 434, 193–204. https://doi.org/10.1016/j.foreco.2018.12.024

Zweifel, R., Drew, D. M., Schweingruber, F., Downes, G. M., Zweifel, R., Drew, D. M., Schweingruber, F., & Downes, G. M. (2014). Xylem as the main origin of stem radius changes in Eucalyptus. Functional Plant Biology, 41(5), 520–534. https://doi.org/10.1071/FP13240

Zweifel, R., Haeni, M., Buchmann, N., & Eugster, W. (2016). Are trees able to grow in periods of stem shrinkage? New Phytologist, 211(3), 839–849. https://doi.org/10.1111/nph.13995

Zweifel, R., Zimmermann, L., & Newbery, D. M. (2005). Modeling tree water deficit from microclimate: An approach to quantifying drought stress. Tree Physiology, 25(2), 147–156. https://doi.org/10.1093/treephys/25.2.147

Zwetsloot, M. J., & Bauerle, T. L. (2021). Repetitive seasonal drought causes substantial species-specific shifts in fine-root longevity and spatio-temporal production patterns in mature temperate forest trees. New Phytologist, 231(3), 974–986. https://doi.org/10.1111/nph.17432

Figure 1.

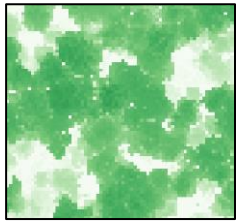

Broadleaf Deciduous Forest (BDF)

Area: 77.6 %

Tree Density: 302 tree ha^{-1}

Species: *Fagus sylvatica*

Quercus petraea x *robur*

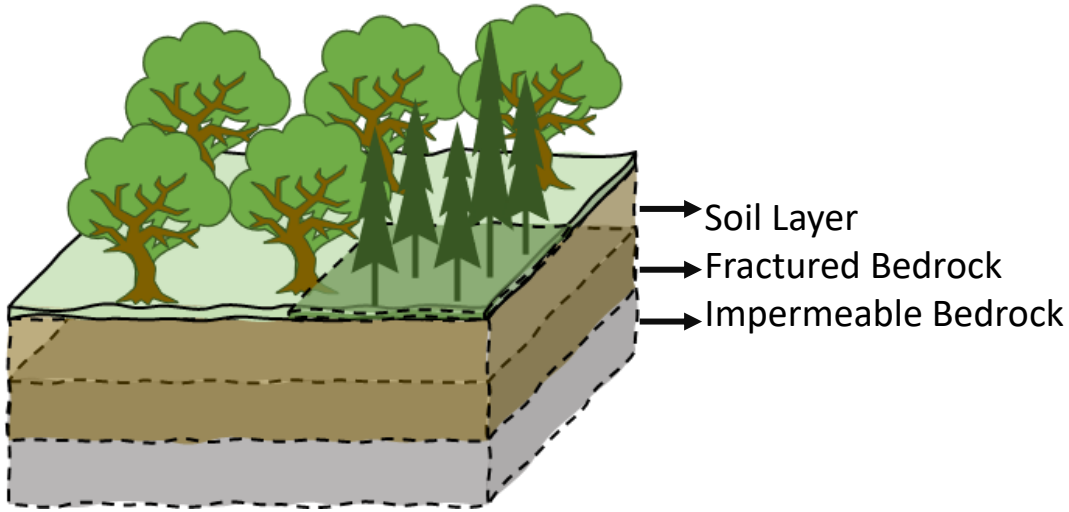

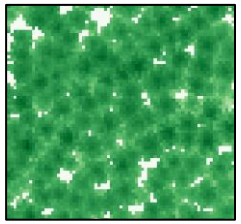

Needleleaf Evergreen Forest (NEF)

Area: 22.4 %

Tree Density: 319 tree ha^{-1}

Species: *Picea abies*

Pseudotsuga menziesii

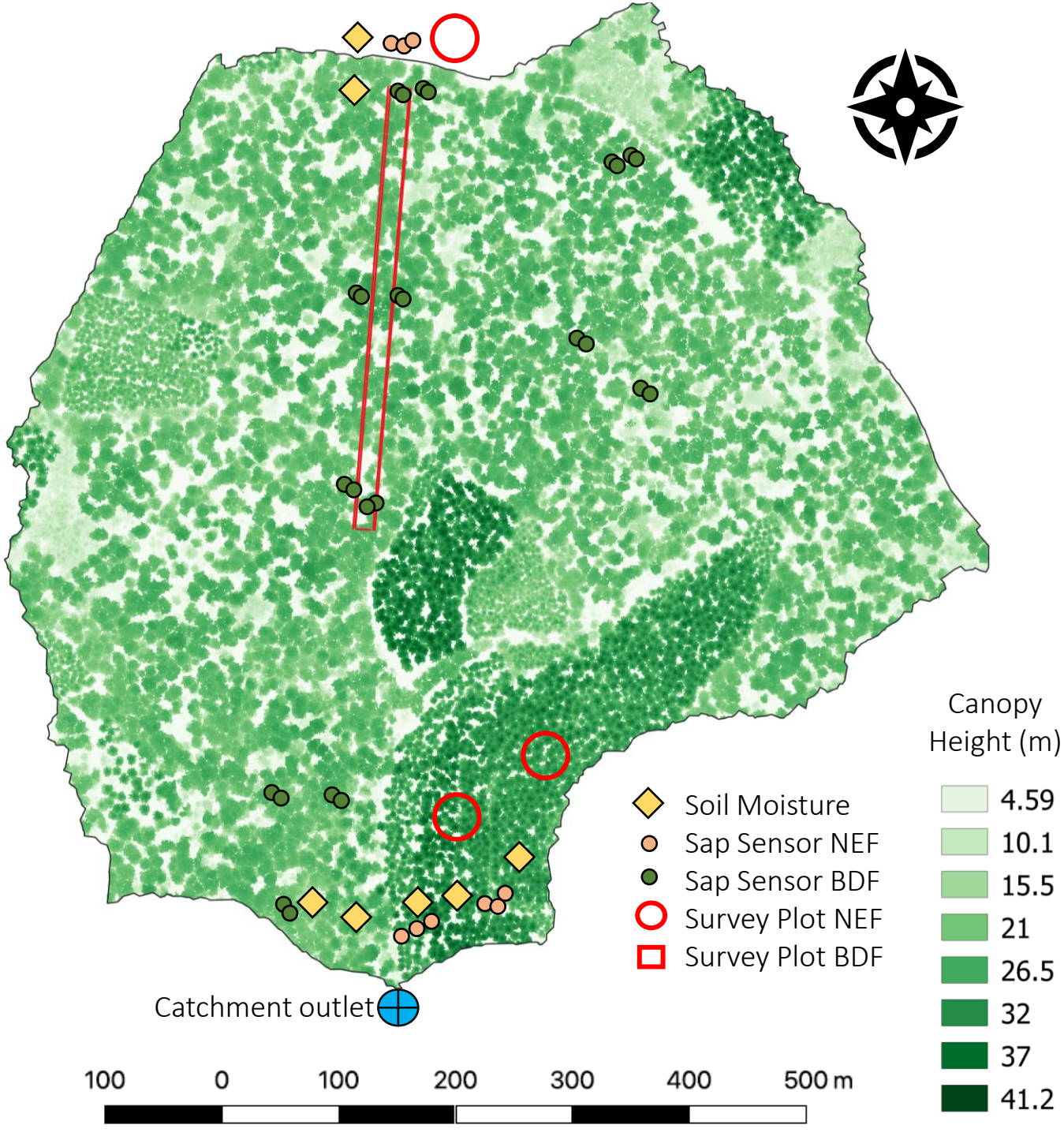

Figure 2.

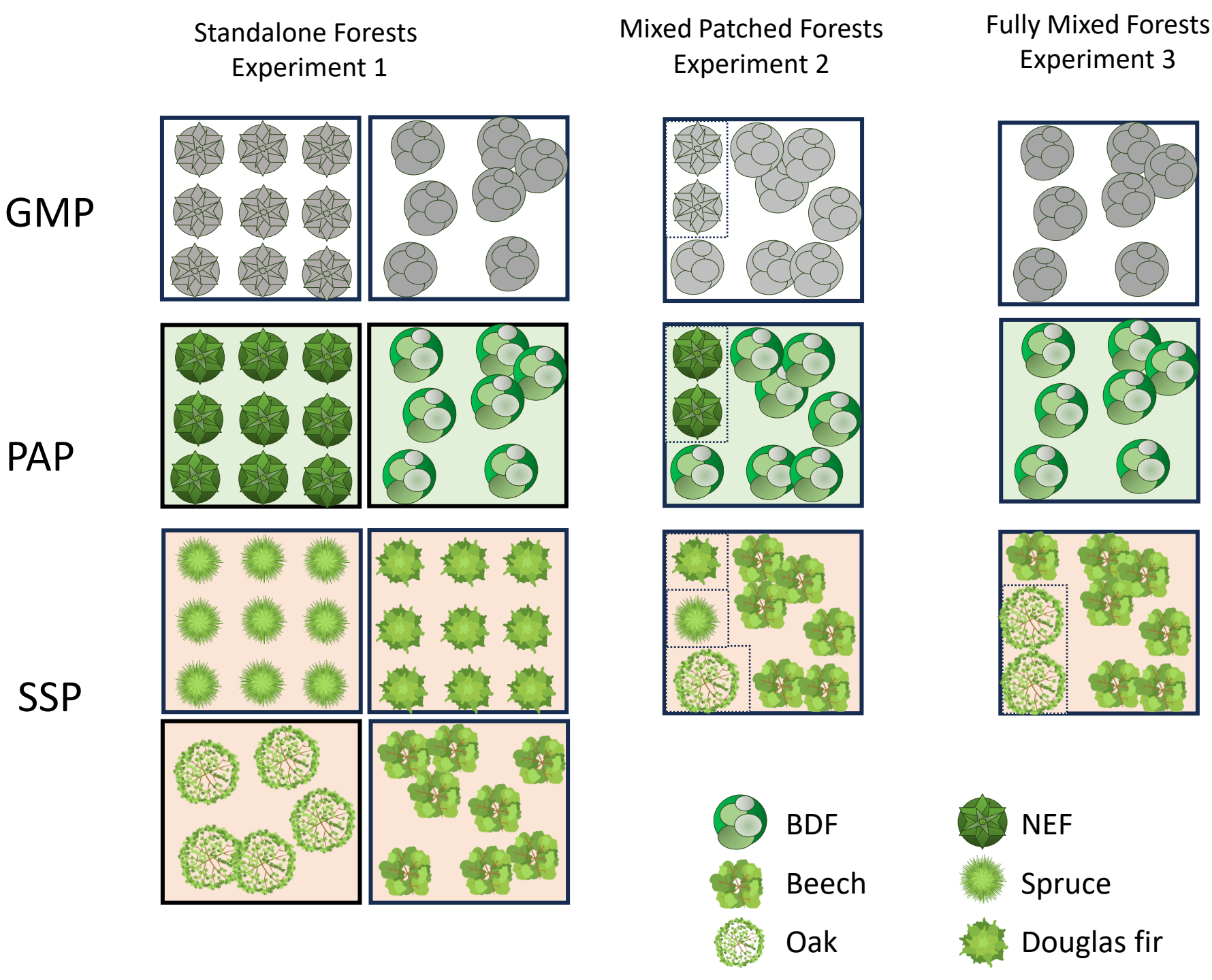
Standalone Forests
Experiment 1
Mixed Patched Forests
Experiment 2
Fully Mixed Forests
Experiment 3
GMP
PAP
SSP
BDF
Beech
Oak
NEF
Spruce
Douglas fir

Figure 3.

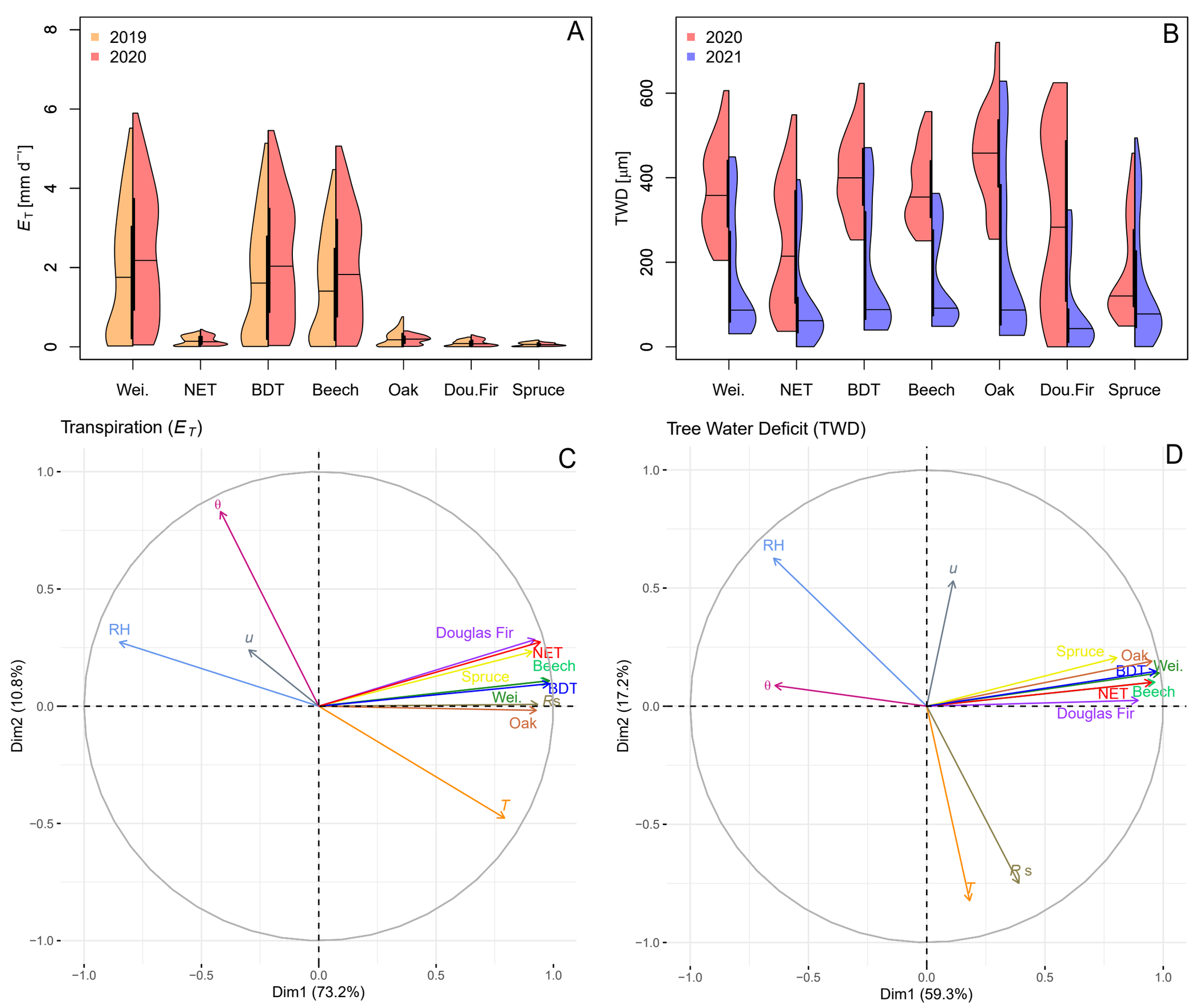
A
2019
2020
E_T [mm d^{-1}]
0
2
4
6
8
Wei.
NET
BDT
Beech
Oak
Dou.Fir
Spruce
B
2020
2021
TWD [µm]
0
200
400
600
Wei.
NET
BDT
Beech
Oak
Dou.Fir
Spruce
Transpiration (E_T)
C
θ
RH
u
Douglas Fir
NET
Beech
Spruce
BDT
Wei.
Rs
Oak
T
Dim2 (10.8%)
Dim1 (73.2%)
Tree Water Deficit (TWD)
D
RH
u
Spruce
Oak
Wei.
BDT
θ
NET
Beech
Douglas Fir
Rs
T
Dim2 (17.2%)
Dim1 (59.3%)

Figure 4.

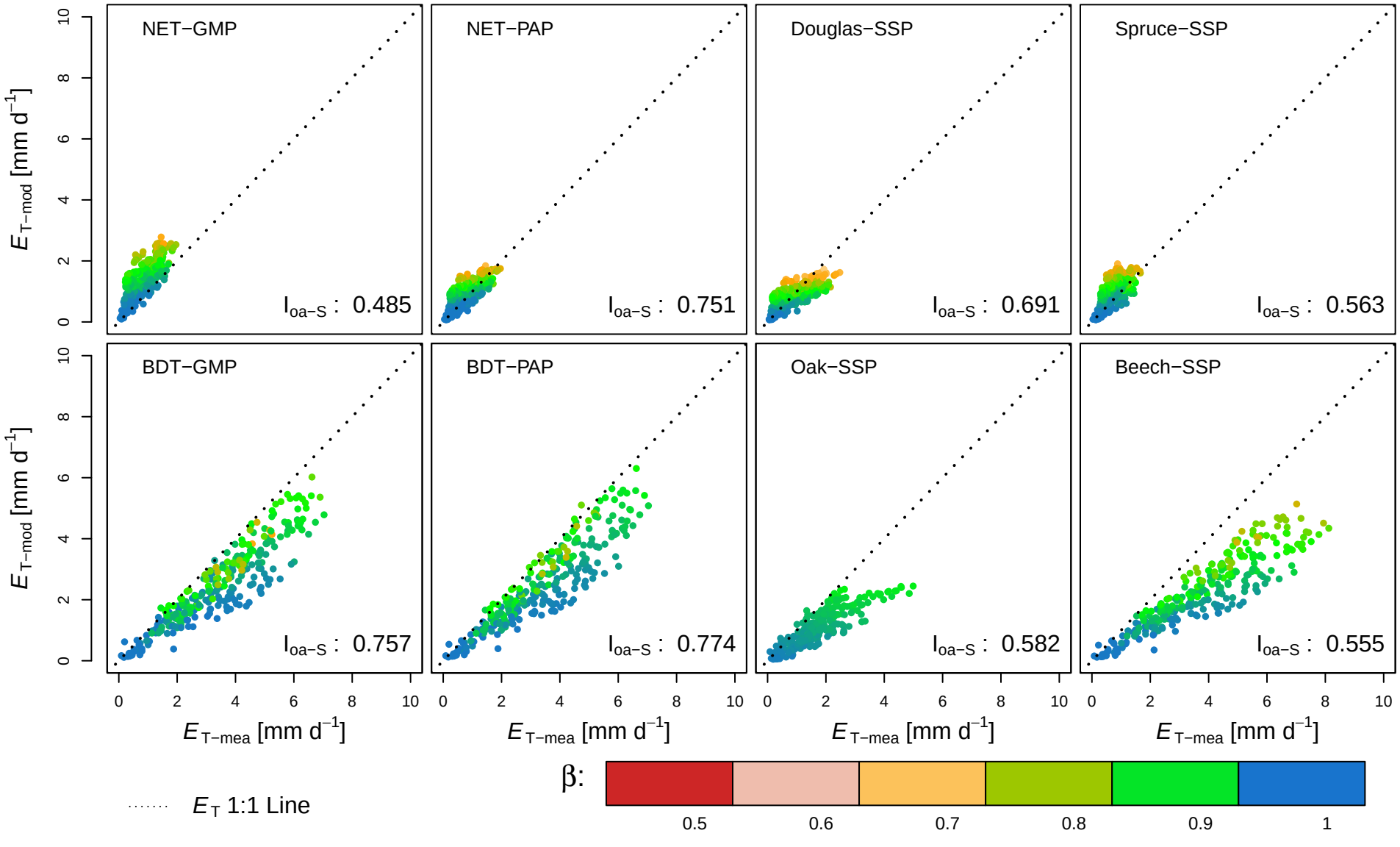
NET−GMP
NET−PAP
Douglas−SSP
Spruce−SSP
BDT−GMP
BDT−PAP
Oak−SSP
Beech−SSP
I_{oa-S} : 0.485
I_{oa-S} : 0.751
I_{oa-S} : 0.691
I_{oa-S} : 0.563
I_{oa-S} : 0.757
I_{oa-S} : 0.774
I_{oa-S} : 0.582
I_{oa-S} : 0.555
E_{T-mod} [mm d^{-1}]
E_{T-mea} [mm d^{-1}]
0
2
4
6
8
10
E_T 1:1 Line
β:
0.5
0.6
0.7
0.8
0.9
1

Figure 5.

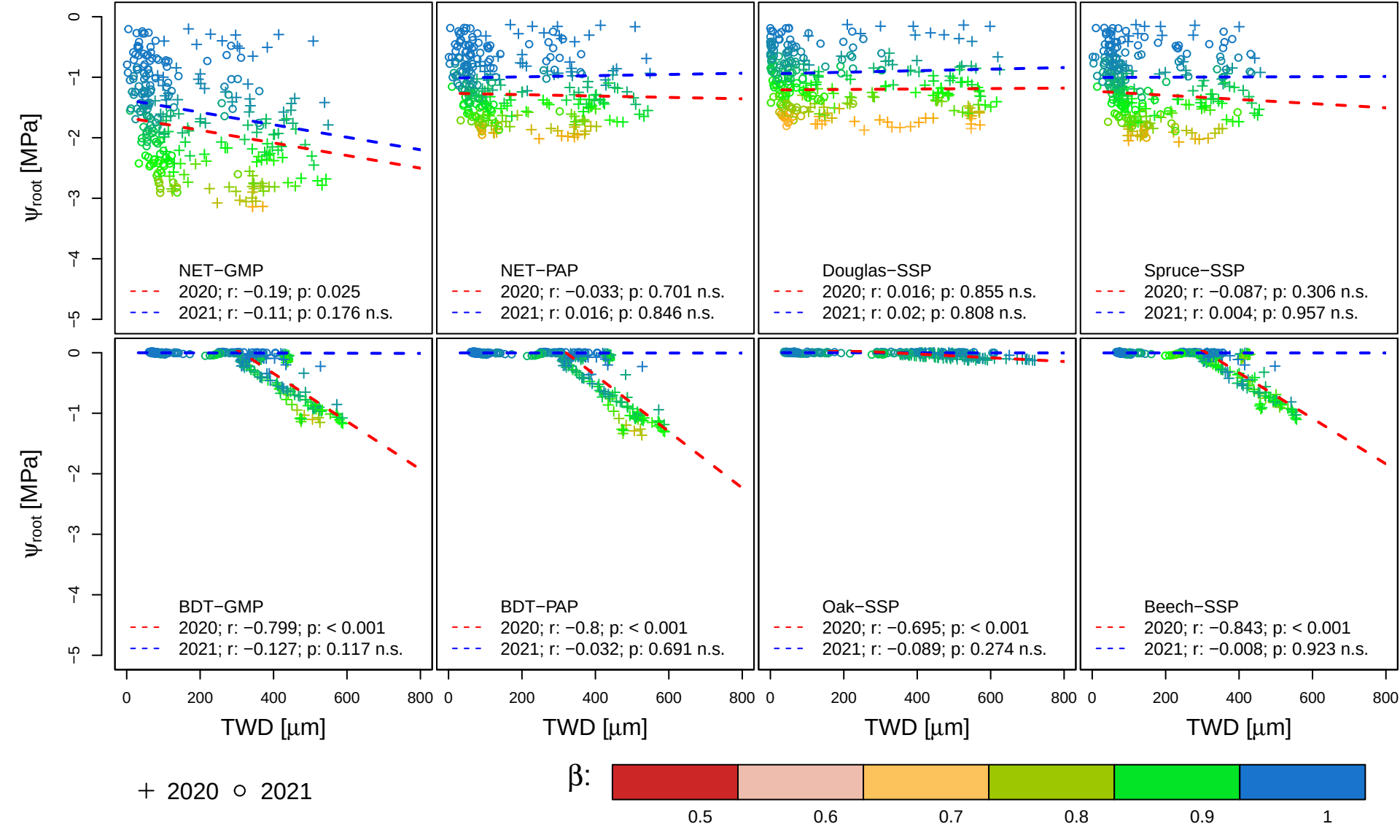
NET−GMP
2020; r: −0.19; p: 0.025
2021; r: −0.11; p: 0.176 n.s.
NET−PAP
2020; r: −0.033; p: 0.701 n.s.
2021; r: 0.016; p: 0.846 n.s.
Douglas−SSP
2020; r: 0.016; p: 0.855 n.s.
2021; r: 0.02; p: 0.808 n.s.
Spruce−SSP
2020; r: −0.087; p: 0.306 n.s.
2021; r: 0.004; p: 0.957 n.s.
BDT−GMP
2020; r: −0.799; p: < 0.001
2021; r: −0.127; p: 0.117 n.s.
BDT−PAP
2020; r: −0.8; p: < 0.001
2021; r: −0.032; p: 0.691 n.s.
Oak−SSP
2020; r: −0.695; p: < 0.001
2021; r: −0.089; p: 0.274 n.s.
Beech−SSP
2020; r: −0.843; p: < 0.001
2021; r: −0.008; p: 0.923 n.s.
ψroot [MPa]
0
−1
−2
−3
−4
−5
0
200
400
600
800
TWD [µm]
+ 2020 ○ 2021
β:
0.5
0.6
0.7
0.8
0.9
1

Figure 6.

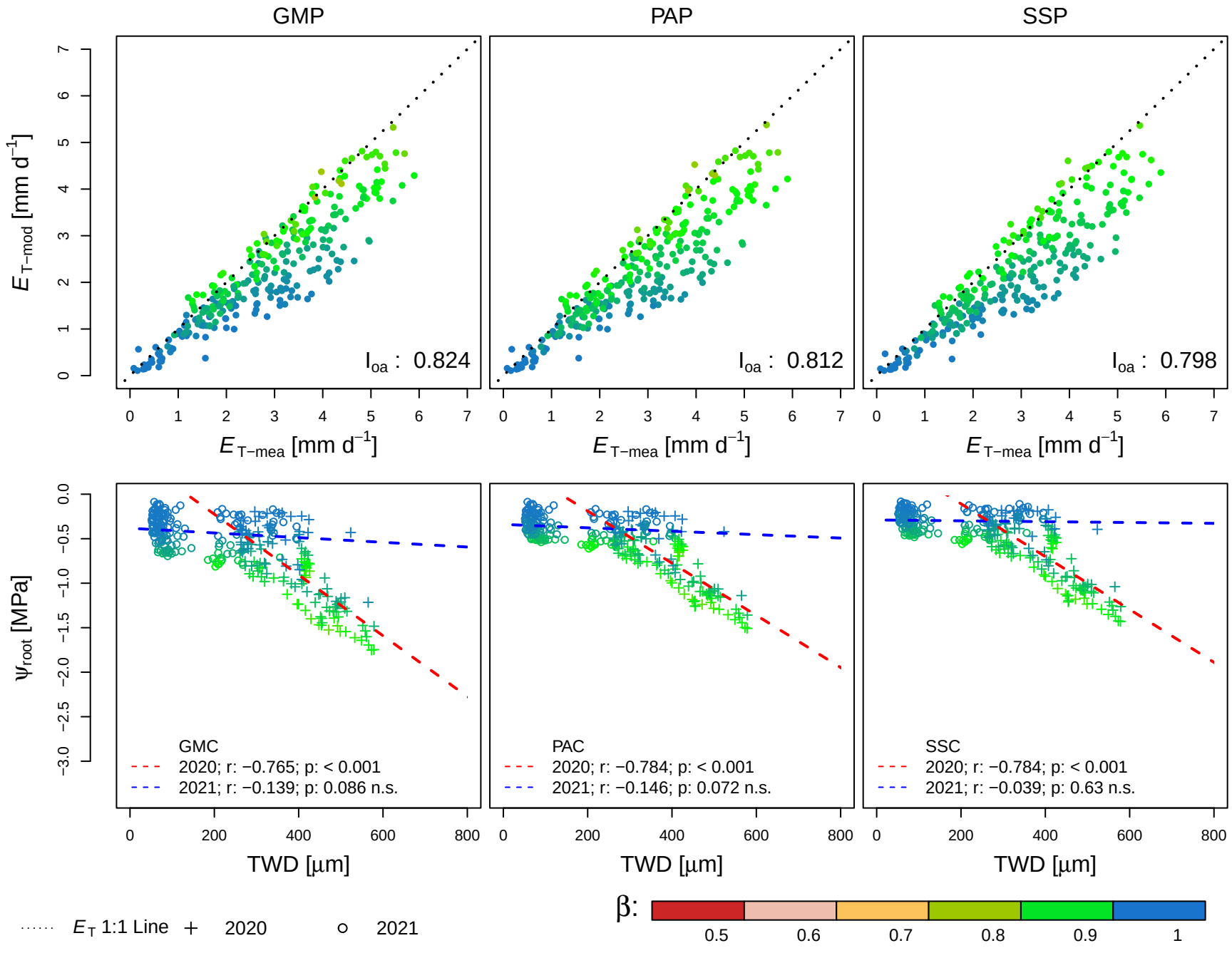
GMP
PAP
SSP
E_{T-mod} [mm d^{-1}]
E_{T-mea} [mm d^{-1}]
I_{oa} : 0.824
I_{oa} : 0.812
I_{oa} : 0.798
ψ_{root} [MPa]
TWD [µm]
GMC
2020; r: −0.765; p: < 0.001
2021; r: −0.139; p: 0.086 n.s.
PAC
2020; r: −0.784; p: < 0.001
2021; r: −0.146; p: 0.072 n.s.
SSC
2020; r: −0.784; p: < 0.001
2021; r: −0.039; p: 0.63 n.s.
E_T 1:1 Line
2020
2021
β:
0.5
0.6
0.7
0.8
0.9
1

Figure 7.

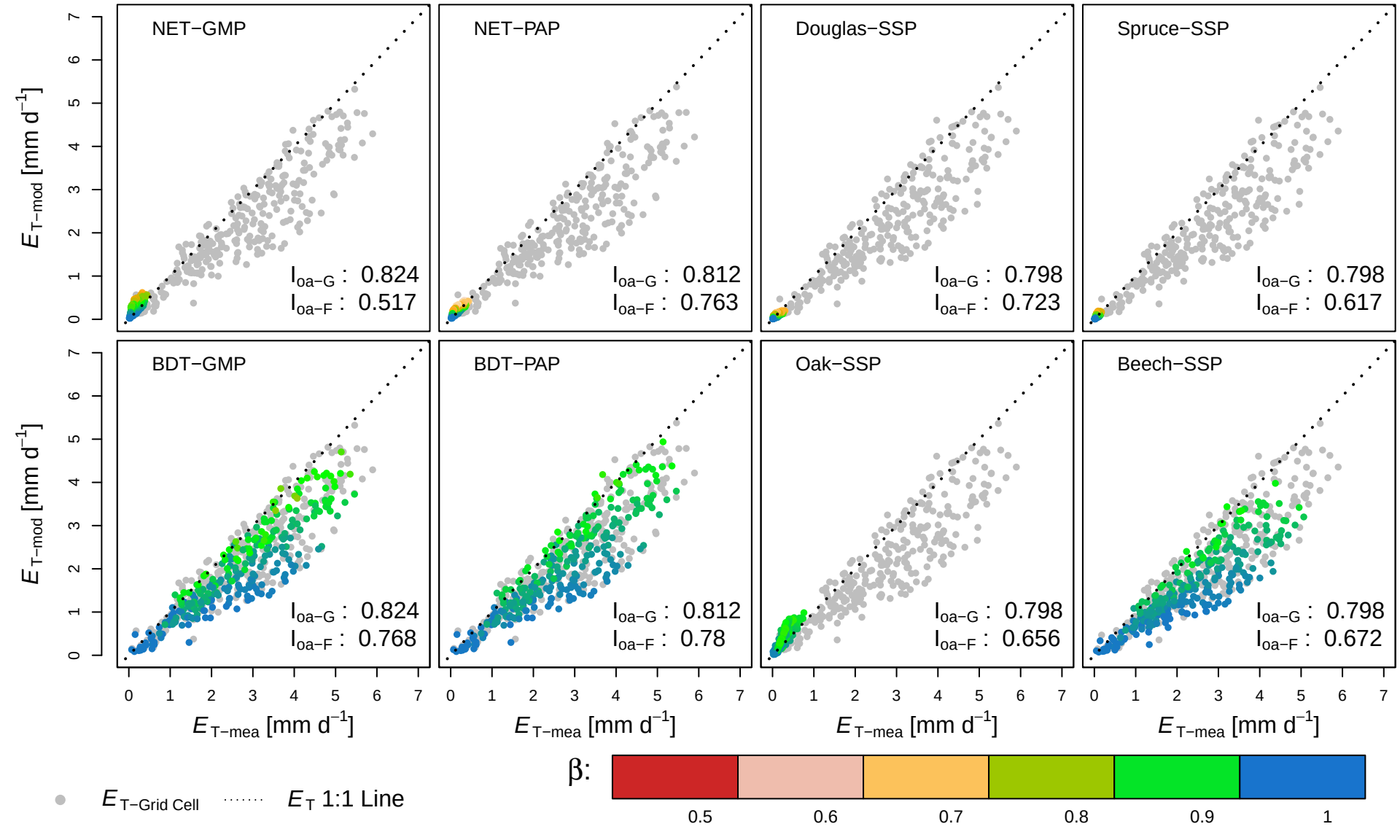
NET−GMP
I oa−G : 0.824
I oa−F : 0.517
NET−PAP
I oa−G : 0.812
I oa−F : 0.763
Douglas−SSP
I oa−G : 0.798
I oa−F : 0.723
Spruce−SSP
I oa−G : 0.798
I oa−F : 0.617
BDT−GMP
I oa−G : 0.824
I oa−F : 0.768
BDT−PAP
I oa−G : 0.812
I oa−F : 0.78
Oak−SSP
I oa−G : 0.798
I oa−F : 0.656
Beech−SSP
I oa−G : 0.798
I oa−F : 0.672
E T−mod [mm d−1]
E T−mea [mm d−1]
0 1 2 3 4 5 6 7
E T−Grid Cell
E T 1:1 Line
β:
0.5 0.6 0.7 0.8 0.9 1

Figure 8.

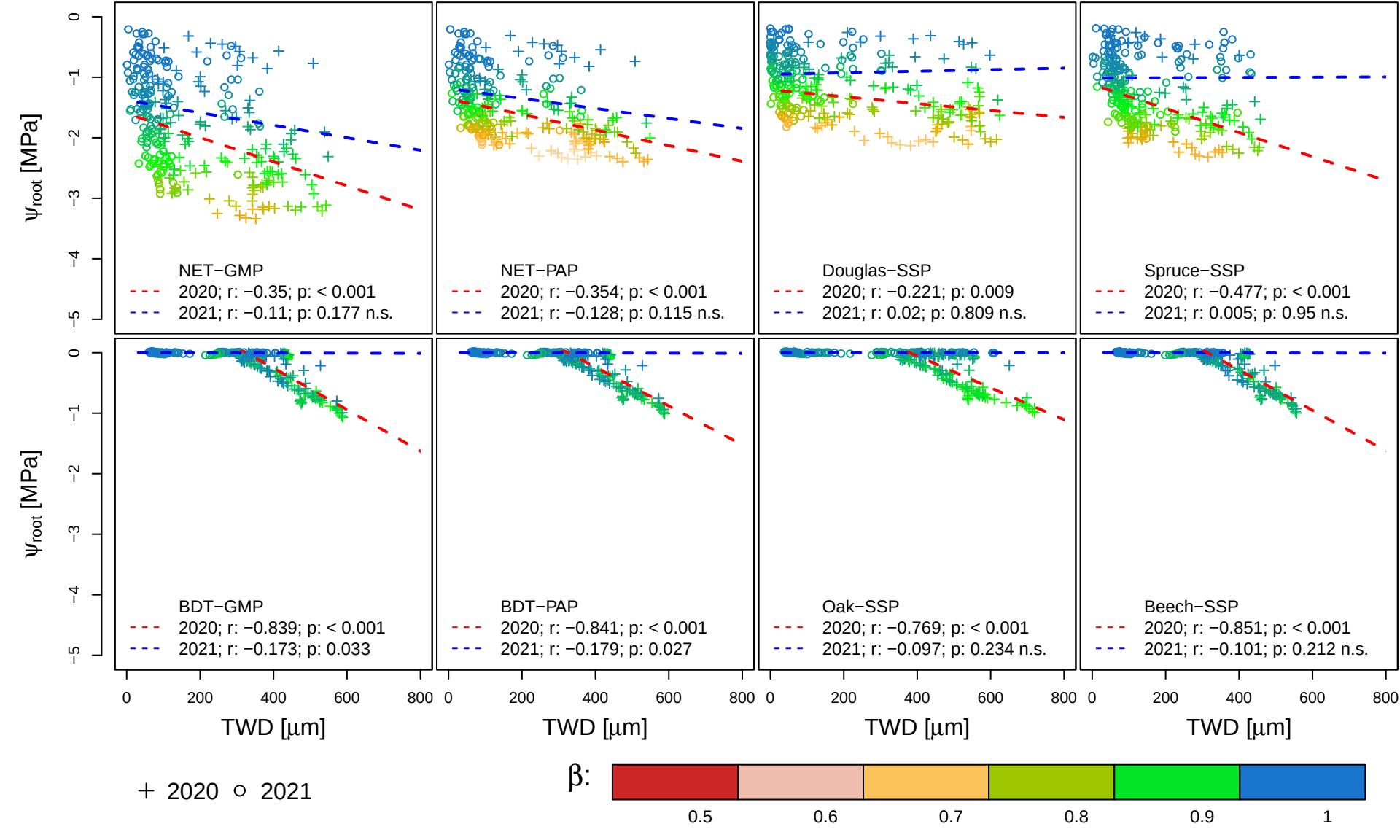
NET−GMP
2020; r: −0.35; p: < 0.001
2021; r: −0.11; p: 0.177 n.s.
NET−PAP
2020; r: −0.354; p: < 0.001
2021; r: −0.128; p: 0.115 n.s.
Douglas−SSP
2020; r: −0.221; p: 0.009
2021; r: 0.02; p: 0.809 n.s.
Spruce−SSP
2020; r: −0.477; p: < 0.001
2021; r: 0.005; p: 0.95 n.s.
BDT−GMP
2020; r: −0.839; p: < 0.001
2021; r: −0.173; p: 0.033
BDT−PAP
2020; r: −0.841; p: < 0.001
2021; r: −0.179; p: 0.027
Oak−SSP
2020; r: −0.769; p: < 0.001
2021; r: −0.097; p: 0.234 n.s.
Beech−SSP
2020; r: −0.851; p: < 0.001
2021; r: −0.101; p: 0.212 n.s.
ψroot [MPa]
TWD [µm]
+ 2020 ○ 2021
β:
0.5
0.6
0.7
0.8
0.9
1

Figure 9.

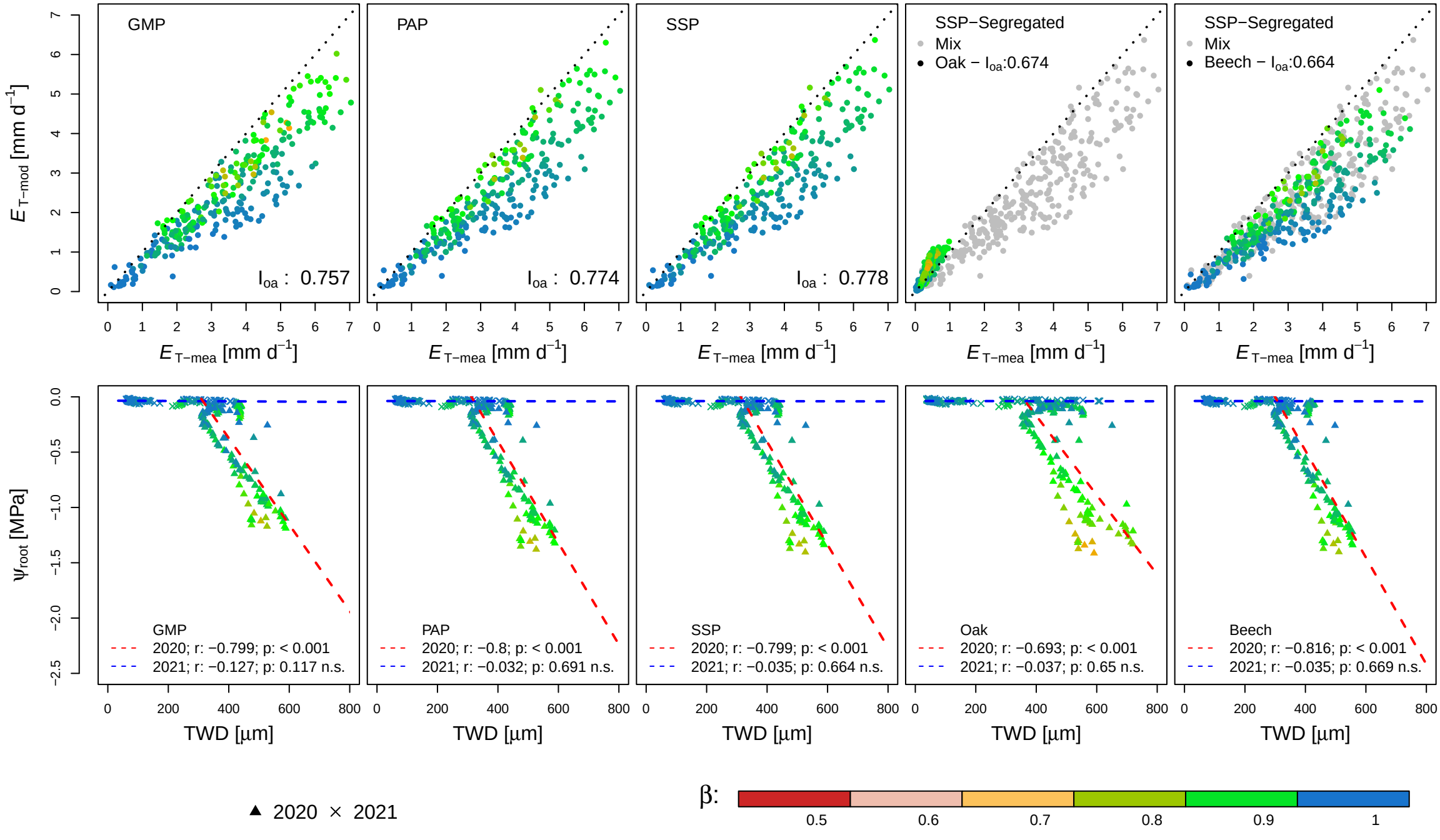
GMP
PAP
SSP
SSP−Segregated
Mix
Oak − Ioa:0.674
SSP−Segregated
Mix
Beech − Ioa:0.664
Ioa : 0.757
Ioa : 0.774
Ioa : 0.778
E T−mod [mm d−1]
E T−mea [mm d−1]
ψroot [MPa]
TWD [µm]
GMP
2020; r: −0.799; p: < 0.001
2021; r: −0.127; p: 0.117 n.s.
PAP
2020; r: −0.8; p: < 0.001
2021; r: −0.032; p: 0.691 n.s.
SSP
2020; r: −0.799; p: < 0.001
2021; r: −0.035; p: 0.664 n.s.
Oak
2020; r: −0.693; p: < 0.001
2021; r: −0.037; p: 0.65 n.s.
Beech
2020; r: −0.816; p: < 0.001
2021; r: −0.035; p: 0.669 n.s.
▲ 2020 × 2021
β:
0.5
0.6
0.7
0.8
0.9
1

Figure 10.

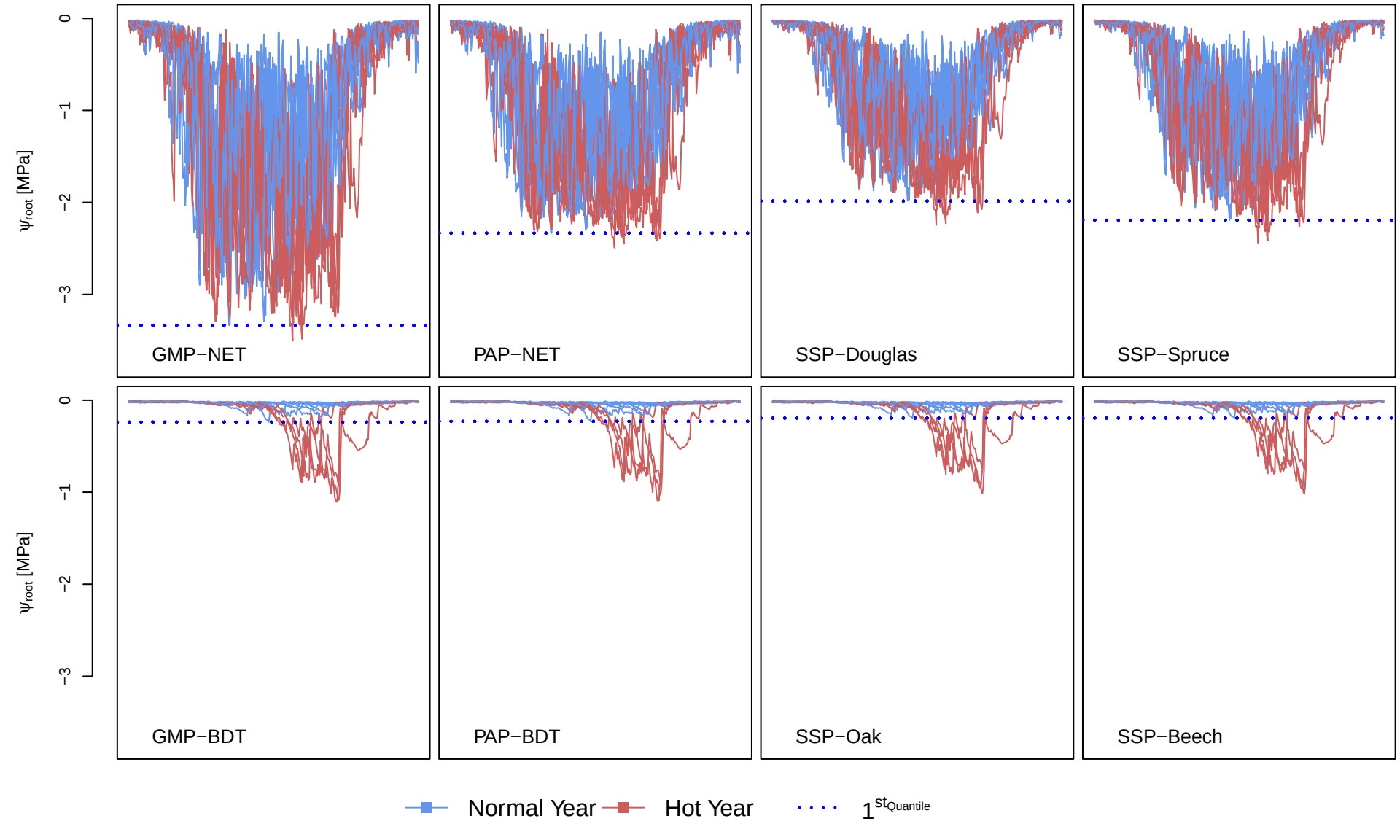
ψroot [MPa]
0
−1
−2
−3
GMP−NET
PAP−NET
SSP−Douglas
SSP−Spruce
GMP−BDT
PAP−BDT
SSP−Oak
SSP−Beech
Normal Year
Hot Year
1stQuantile